Chapter 1

Introduction

1-1 Overview of Low-Temperature Polycrystalline-Silicon (LTPS) Thin-Film Transistors (TFTs) Technology

Nowadays, the amorphous silicon thin film transistors (a-Si TFTs) are commonly used to be the switches of the pixel in active matrix liquid crystal displays (AMLCDs). Fig. 1-1. shows the block diagram of active matrix display. All the driver chips are buried together with the other application-specified ICs on PCB because the current driving capacity of a-Si TFTs is not good enough for the system integration. However, the integration of driver circuitry with display panel on the same substrate is very desirable not only to reduce the module cost but to improve the system reliability. For this reason, the polycrystalline silicon thin-film transistors (poly-Si TFTs) have attracted much attention in the application of the pixel circuits and the integrated peripheral circuits of active matrix liquid crystal displays (AMLCDs) [1]-[8] due to its high electron mobility. In poly-silicon film, the carrier mobility larger than 10 cm^2/Vs can be easily achieved, which is about tens times larger than that of the conventional amorphous-silicon TFTs (typically below 1 cm^2/Vs). This characteristic allows the pixel-switching elements made by smaller TFTs size, resulting in higher aperture ratio and lower parasitic gate line capacitance for the improvement of display performance. Furthermore, the integration of peripheral circuits in display electronics can be achieved by poly-Si TFTs due to its higher current driving capability, which is illustrated in Fig. 1-2. Besides, it can offer the flexibility of being used in the peripheral driving circuitry of AMLCD panel [9]-[12] to achieve the goal of system-on-panel (SOP) which is the integration of all the components on the same glass substrate, such as active displays, driving circuits, memory, and central processing unit (CPU), etc.

In the process of fabricating LTPS TFTs (Low Temperature Poly-Si Thin Film Transistors), crystallization of a-Si has been considered the most important procedure

for excellent performance of TFTs. To achieve high performance poly-Si TFTs, high quality poly-Si thin film is firstly required. It is known that the existence of traps in poly-Si thin film has great impact on the electrical properties of poly-Si TFTs. The conductivity of poly-Si TFT is mainly influenced by the grain boundaries because the trap levels at the grain boundaries form the potential barrier. However, diverse grain boundary distribution in poly-Si film also leads to the non-uniformity of device characteristics and the difficulty in predicting the reliability behavior [13]-[15]. Therefore, the yield control of the poly-Si TFTs is very difficult due to the poor uniformity of poly-Si TFTs compared with single crystal silicon transistors. In this work, the device characteristics are studied in a statistical approach to investigate the relationship between variation behavior and layout methods in the low-temperature poly-silicon films.

1-2 Review of Mismatch Effects in LTPS TFTs

1-2-1 Device variation

In previous research, it is shown that the LTPS TFTs have some non-ideal characteristics such as device variation and diverse reliability behaviors. Until to the present time, very few researches have been made on the variation issue of LTPS TFTs. Most researches about LTPS TFTs aim at the improvement of the device performance. The LTPS TFTs suffer from serious variation of their electrical parameters [16]-[18]. The poly-Si material is a heterogeneous material made of very small crystals of silicon atoms in contact with each other constituting a solid phase material. These small crystals are called crystallites or grains. The irregular boundaries of these crystallites are the side lines of the grains. Because the material remains solid, the atoms at the border of a crystallite are also linked to the neighbor

crystallite ones. However, these atom bonds are disoriented in comparison with a perfect lattice of silicon. This border is called a grain boundary. As the result of various distributions of grain boundaries in the channel of TFTs, the initial characteristics of LTPS TFTs are different from one another. These variations can be also observed in MOSFETs (Metal-Oxide-Silicon Field Effect Transistors) but they are more critical in LTPS TFTs due to the existence of grain boundary. The device variation will lead to the variation of the circuit performance. It will be reflected directly on the image uniformity of the display. This lack of uniformity has hindered the adaptation of polycrystalline TFT's (poly-TFT's) in the key applications mentioned above. It would be useful if a theory existed to quantify this variation. Although changes in TFT uniformity are expected when the devices are scaled, conventional MOS scaling theory was not intended to address such changes. There has been some research into addressing of TFT's variation. Uncontrolled variations tend to become dominant at small device sizes. They require device or circuit designer to improve uniformity.
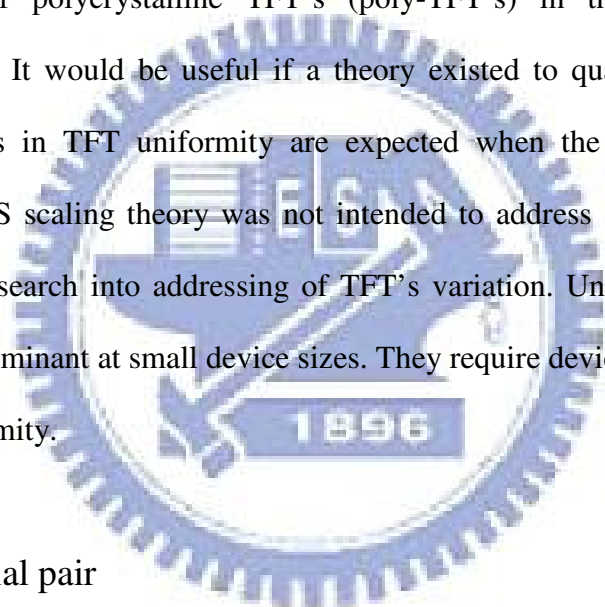
1-2-2 Differential pair

The objective of matching two or more devices on a single integrated circuit is depicted in Fig. 1-3. If a circuit critically depends on the absolute performance of a single transistor, the circuit will vary according to the die-to-die variation. On the other hand, if a circuit is designed so that it depends on the differential performance of a matched pair, the circuit becomes robust to die-to-die variation and instead it depends on a much smaller "mismatch" variation. The extent to which two or more identically drawn devices match each other therefore determines parametric yield, analog circuit performance (such as bit resolution in data converters), and circuit topology selection.

The circuit performance of an analog circuit, such as differential pair is dominated by micro variation of devices. The differential amplifier is among the most important circuit inventions, dating back to the vacuum tube era. Offering many useful properties, differential operation has become the dominant choice in today's high-performance analog and mixed-signal circuits. An important attributes of differential amplifiers is their ability to suppress the effect of common-mode perturbations. In a symmetric circuit, input CM (common-mode) variations disturb the bias points, altering the small-signal gain and possibly limiting the output voltage swings. However, considering the asymmetry resulting from mismatches between M_1 and M_2 in Fig. 1-4(a), the two transistors would carry slightly different currents and exhibit unequal transconductances, which owes to the mismatches of dimension and threshold voltage.

It is a valid argument that the value of CMRR (common-mode rejection ratio) decrease as the mismatches between the two transistors get worse, which means that the differential amplifier has worse tolerance with signal's fluctuation. Therefore, it is obvious that the study of the matching behavior of MOS transistors remains important because the performance of analog MOS integrated circuits depends heavily upon the element of matching accuracy.

1-2-3 Mismatch issue

It is generally agreed that the mismatching variations in IC design are further extended as wafer-to-wafer, batch-to-batch and lot-to-lot variation. The mismatch issue is examined with respect to the mutual device distance. In the application using MOSFETs with high sensitivity to the mismatch variations such as differential amplifiers, the statistical mismatching analysis would be a very important verification step. In the scope of this thesis, since the LTPS TFTs may be used to make advanced

circuitry and the perspective of System-On-Glass (SOG), the mismatch and uniformity issue would become more essential.

There is no disagreement that LTPS TFTs have different process from IC industry owing to the different substrate and low process temperature, which could be the source of the device's mismatching behavior. Besides, compared with MOSFETs, the LTPS TFTs contains a larger number of defects in the poly-silicon film as shown in Fig. 1.5, which distributes randomly and hardly controlled by manufacturing process. Therefore, it may farely be assumed that the mismatching effect on LTPS TFTs could be more essential and complicated than that on MOSFETs [19].

Mismatch sources of LTPS TFTs can be divided as local variations characterized by short correlation distances and global variations characterized by long correlation distances, where the correlation distance is defined as the distance in which a process disturbance affects the device performance. If this distance is lower than the usual distance between devices, the disturbance constitutes a local variation and affects few devices (e.g. a charge trapped in the gate oxide layer). For the global variation, which is characterized by process disturbances with longer correlation distances (e.g. the gate oxide thickness across the wafer surface), affects all the devices within a defined region. Therefore, the devices placed at longer distance are more affected by global variations than devices placed close to each other.

In this work, the sources of mismatch are classified as macro variation and micro variation. Macro variation comes from the issue of process control, such as gate insulator thickness, LDD (Lightly Doped Drain) length fluctuation and ion implantation uniformity. This non-uniformity of process control will result in the common shift of device parameters. On the other hand, micro variation comes from the differences of the defect site, defect density in the active region and the activation efficiency. Since these conditions vary from device to device, micro variation will

lead to the random distribution of device parameter.

We will introduce the crosstie layout device which was used to investigate the mismatching properties in chapter two. In chapter three, the mismatch issue of LTPS TFTs will be discussed with the distribution of device parameters. We will investigate the correlation between the channel width and the micro variation. Our experimental data tell us that the larger channel width the devices have, the smaller the micro variation there will be. How about the micro variation of the smaller channel width devices will be? We are interesting in the micro variation of the smaller channel width, and in chapter four, we will use the simulation to evaluate it.

1-3 Thesis Outline

Chapter 1-Introduction

1-1   Overview of Low-Temperature Polycrystalline-Silicon Thin-Film Transistors
        (LTPS) Technology

1-2   Review of Mismatch Effects in LTPS TFTs

        1-2-1 Device Variation

        1-2-2 Differential Pair

        1-2-3 Mismatch Issue

1-3   Thesis Outline

Chapter 2-Experiments

2-1   Introduction to Crosstie TFTs

2-2   Device Fabrication and Measurements

2-3   Parameter Extration

2-4   Statistical Analysis

Chapter 3. Mismatch Analysis Based on Measurement Data
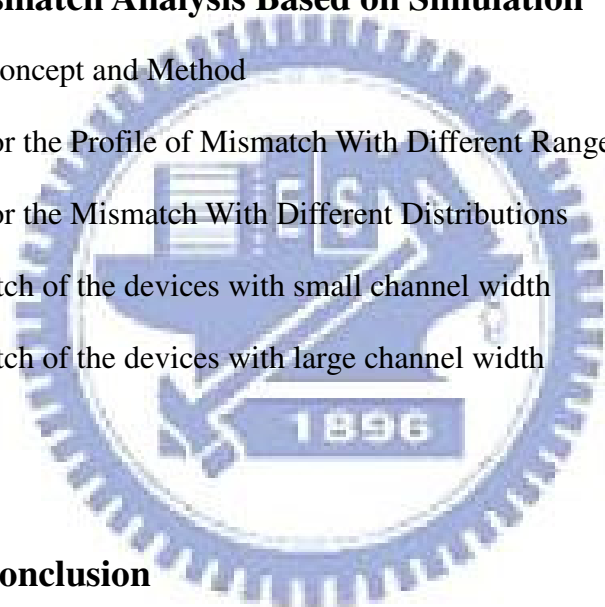
Chapter 4. Mismatch Analysis Based on Simulation

Chapter 5.   Conclusion

References

Figures

Tables

Chapter 2

Experiments

2-1   Introduction to Crosstie TFTs

To further investigate the mismatching properties of the interdigitated arrangements, a huge number of devices with the same dimension are necessary. In addition, the variation factors in LTPS TFTs needs to be considered to evaluate the mismatching property more precisely.

In prior studies, it is known that LTPS TFTs suffered from severe device variation even under well-controlled process. Since the device variation is inevitable in LTPS TFTs, it is essential to classify the sources of variation. In MOSFETs (Metal-Oxide-Silicon Field Effect Transistors), the local variations can be characterized by short correlation distances and global variations characterized by long correlation distances, where the correlation distance is defined as the distance in which a process disturbance affects the device performances. If this distance is lower than the usual distance between devices, the disturbance constitutes a local variation and affects few devices (e.g. a charge trapped in the gate oxide layer). For the global variation, which is characterized by process disturbances with longer correlation distances (e.g. the gate oxide thickness across the wafer surface), affects all the devices within a defined region. Therefore, the devices placed at longer distance are more affected by global variations than devices placed close to each other.

In order to investigate the relationship between mismatching issue and device distance, a special layout of the devices adopted in this work is shown in Fig. 2-1(a). The red, blue and yellow regions respectively represent the polysilicon film, the gate

metal and the source/drain metal. The structure of the poly-Si film and the gate metal are in the order that resembles the crosstie of the railroad and therefore this layout is called the crosstie type layout of LTPS TFTs. The distance of two nearest active regions is equally-spaced 40µm and is shown in Fig. 2-1(b). The global variation may be ignored within this small distance, and the variation of device behavior can therefore be reduced to only local variation. For this reason, we can find out the relationship between the variation behaviors and the distance of mutual devices by adopting the crosstie layout TFTs.

2-2   Device Fabrication and Measurements

Since the uniformity of polycrystalline TFT's is expected to be worse than that of MOS transistors qualitatively, the mismatching behaviors that can be observed between the electrical characteristics of equally designed devices are further analyzed by means of equally designed devices with various dimensions.

The process flow of top gate LTPS TFTs is described below. Firstly, the buffer oxide and a-Si:H films with thickness of 50 nm were deposited on glass substrates with PECVD. The samples were then put in the oven for dehydrogenation. The XeCl excimer laser of wavelength 308 nm and energy density of 400 mJ cm^{-2} was applied. The laser scanned the a-Si:H film with the beam width of 4 mm and 98% overlap to recrystallize the a-Si:H film to poly-Si. After poly-Si active area definition, 100 nm SiO$_2$ was deposited with PECVD as the gate insulator. Next, the metal gate was formed by sputter and then defined. For n-type devices, the lightly doped drain (LDD) and the n+ source/drain doping were formed by PH$_3$ implantation with dosage 2×10^{13} cm^{-2} and 2×10^{15} cm^{-2} of PH$_3$ respectively. The LDD implantation was self-aligned and the n+ regions were defined with a separate mask. The LDD structure

did not use on p-type devices. The p+ source/drain doping was done by B_2H_6 self-align implantation with a dosage of 2×10^{15} cm^{-2}. Then, the interlayer of SiNx was deposited. Subsequently, the rapid thermal annealing was conducted to activate the dopants. Meanwhile, the poly-Si film was hydrogenated. Finally, the contact hole formation and metallization were performed to complete the fabrication work. The Fig. 2-2. shows the schematic cross-section structure of the n-type poly-Si TFT with lightly doped drain (LDD). And the Fig. 2-3. shows the schematic cross-section structure of the p-type poly-Si TFT.

In order to realize the matching properties of LTPS TFTs, the I-V curves of the TFTs were measured using an HP 4156 semiconductor parameter analyzer. The maximum field-effect mobility was extracted from the transconductance in the linear region at Vds= -0.1V. The minimum subthreshold swing were measured at Vds = -0.1 V and the threshold voltage was defined as the gate voltage required to achieve a normalized drain current of Ids = (W/L)*10^{-8} A at Vds = -0.1 V.

2-3 Parameter Extraction

The purpose of this section is to introduce the definition of estimating the key parameters threshold voltage (Vth), field effect mobility (Muo) and subthreshold swing (S.S) from measured data obtained from the I-V characteristics, including the operation on tride and saturation region.

For most of the researches on TFT, the constant current method is widely-used to determine the threshold voltage (Vth). The threshold voltage in the thesis is determined from this method, which extracts Vth from the gate voltage at the normalized drain current $I_N = I_D/(W_{eff}/L_{eff}) = 10nA$ for VD=0.1V.

The field effect mobility (Muo) is derived from the transconductance gm. The transfer characteristics of poly-Si TFTs are similar to those of conventional MOSFETs, so the first order I-V relation in the bulk Si. The MOSFETs can be applied to the poly-Si TFTs, which can be expressed as

$$I_D = \mu_{FE} C_{ox} \frac{W}{L} [(V_G - V_{th})V_D - \frac{1}{2}V_D^2]$$

(2-1)

Where

Cox is the gate oxide capacitance per unit area,

W is channel width,

L is channel length,

Vth is the threshold voltage.

If the drain voltage VD is much smaller compared with $V_G - V_{th}$

(i.e. VD << VG - Vth), then the drain current can be approximated as:

$$I_D = \mu_{FE} C_{ox} \frac{W}{L} (V_G - V_{TH})V_D$$

(2-2)

And the transconductance is defined as:

$$g_m = \frac{\partial I_D}{\partial V_G}\bigg|_{V_D = const.} = \frac{WC_{ox}\mu_{FE}}{L}V_D$$

Therefore, the field effect mobility can be expressed as:

$$\mu_{FE} = \frac{L}{C_{ox}WV_D} g_m$$

(2-3)

We can get the field-effect mobility by taking the maximum value of the gm into (2-3) when VD = 0.1V.

2-4　Statistical Analysis

It is reported that the averages of parameters differences stand for global variation of LTPS TFTs, while the standard deviation of parameter differences shows the local variation in the devices. In prior art, the averages of the differences of these parameters show different behaviors, they still appear in linear form. On the other hand, the effects of variation in a range are still minor than those of the micro variation under short device distance. Since the variation in a long range is not our concern because the distance between two devices will not be too long for the crosstie layout. A good place to start is analyzing the distribution of the differences of these parameters.

Since the crosstie devices queues as a row with narrow distance of 40um, it can be used for statistical method to analyze the mismatch effect. In this study, the crosstie devices are interdigitated with different numbers of fingers. In order to compare the performance of the interdigitated pairs and the original ones, the value of the drain currents within the same pair are summed together and extracted to acquire the two parameters of threshold voltage and mobility. To further confirm the matching properties of the interdigitated pairs, the crosstie devices could be interdigitated not only with different number of fingers, but also with different distance of fingers. By employing various arrangements of the interdigitated pairs, the property of mismatch effect can be further analyzed and evaluated.

2-4-1 Average and Standard deviation

Firstly, we introduce the statistical expressions for the following analysis. The average value (μ) is defined as:

$$\bar{X} = \frac{\sum\limits_{i=1}^{n} x}{n}$$, where x is the observe value (2-4)

The standard deviation value, σ, is usually used to investigate the distribution of the observed value. The standard deviation value is given as

$$\sigma \equiv \sqrt{\frac{1}{n}\sum_{n}\left(x-\bar{X}\right)^2}$$, where x is the observe value (2-5)

2-4-2 Inter-quartile Range

Because the range depends only on the smallest and largest observations in a data set, a modified range is sometimes used that reflects the variability of the middle 50 percent of the observations in the array. This modified range is called the inter-quartile range. The inter-quartile range is the difference between the third and first quartiles of the data set. The inter-quartile range may be considered to be approximately the range for a trimmed data set in which the smallest 25 percent and the largest 25 percent of observations have been removed.
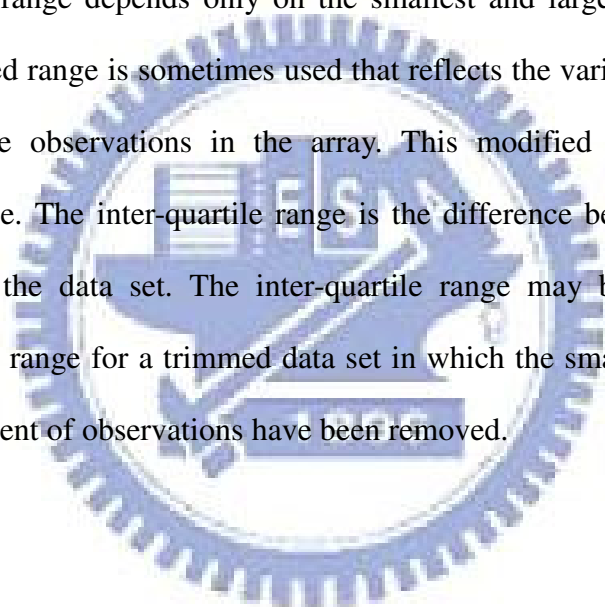
Chapter 3

Mismatch Analysis Based on Measurement Data

3-1 The Distribution of the Device Parameter Mismatch

As mentioned in chapter 1-2-1, LTPS TFTs are found to suffer serious behaviors of mismatching variations even from predominant process conditions. Fig. 3-1-1 illustrates the threshold voltage distribution along the device position. We can take this graph as a part of Fig. 3-1-2, which is the same kind of graph but in longer distance. The variation effects consist of macro and micro variations, but it mainly comes from the macro variation. The macro variation results from the issues of process control, such as gate insulator thickness, LDD length fluctuation and ion implantation uniformity. This non-uniformity of process control will lead to the common shift for device parameters. On the other hand, micro variation may result from the difference of the defect site, defect density in the active region and the activation efficiency. Since these conditions differ from device to device, the micro variation will lead to the random distribution of device parameters. In order to identify the effects of the macro and micro variation, the parameters differences of two devices under certain distance are divided with several groups according to the distance between two devices. Fig. 3-1-3 and Fig. 3-1-4 show the average and the standard deviation of the differences of Vth and Mu of Poly-GroupA and Poly-GroupB devices. As the mutual device distance increases, the standard deviation of device differences shows no significant dependence on the device distance. It can be explained that the micro variation will merely vary with distance as we expect. On the other hand, as for the variation in a range, the averages of the differences of these

parameters change with the mutual device distance. In the very linear region, the effects of the macro variation can be minor than those of the micro variation .

For the viewpoint of circuit design, the device variation must be taken into consideration. Analogy to the small signal analysis in the circuit theory, the macro variation can be considered as the range near the bias point and appear in piecewise linear form, while the micro variation can be taken as the noise. If the distance between devices is short enough, the disturbance constitutes a micro variation and thus the macro variation can be ignored. For this reason, we can evaluate the micro variation individually if we keep the mutual device distance close. This is our aim that to eliminate the macro variation effects and just focus on the micro variation on our analysis.

3-2 Scaling Effect of the Mismatch

It is reported that the improved grain structure of the TFT's with small channel dimensions may be related to the decrease in the number of grain boundaries in the active channel of the devices [21]. Furthermore, these results reveal that the difference of output decrease with larger device size. Uncontrolled variations tend to become dominant at small device sizes. However, if the channel width increases so much that not only the micro variation is involved, the macro variation will also come into play.

In order to eliminate the macro variation while the device size increasing, we use the interdigitated layout. As mentioned in chapter 2-1, the distance between device pair of interdigitated layout is not too long. By cancelly out the common variation factors of the two matched devices, the major variation source in the circuits is micro variation. By putting matched devices in parallel, we can scale up the device size while not incorporating the macro variation.

We show the p-type and the n-type channel devices for Poly-GroupA device. In

order to evaluate the performance of the interdigitated pairs, more than 1000 crosstie

devices are measured and interdigitated statistically with different setup as illustrated

in Fig. 3-2-1. According to the device parameters extracted from the measured data,

the distributions of the parameters' difference including threshold voltage and

mobility are observed. The mean values and standard deviations of each distribution

for various kinds of interdigitated methods are examined. Fig 3-2-2 (a), (b) and (c)

shows the distribution of $\triangle$Vth of n-type devices with 1, 2, and 3 fingered in pairs

respectively. The number of fingers also means the size of devices in the interdigitated

pair. In Fig. 3-2-2(a), the threshold voltage's difference of one finger devices spread

out as Gaussian distribution, whose mean value and standard deviation are -0.009mV

and 0.022V individually. In the cases of multi-finger, the distributions are still

Gaussian and the mean values keep near 0mV, as shown in Fig 3-2-2 (b), and(c).

However, the standard deviations of two-finger and three-finger interdigitated devices

decrease linearly with the value of 0.015V and 0.012V. Observing the decrease of

standard deviation, it is not too far to say that the interdigitated method is able to

suppress the mismatch effect with the increase of finger number.

Since the interdigitated method shows superior properties on $\triangle$Vth parameter in

n-type Poly-GroupA devices, the performances on $\triangle$Mu are intended to be examined.

The distribution of $\triangle$Mu, in each finger group, are shown in Fig 3-2-3 (a), (b) and (c)

accordingly. In these three distributions, the mean values of -0.0028 cm^2/V*s, -0.0025

cm^2/V*s, and -0.0033 cm^2/V*s, are very close to zero, while the standard deviation

shows more apparent decrease with the value of 1.811 cm^2/V*s, 1.361 cm^2/V*s and

1.158 cm^2/V*s. As far as the standard deviation is concerned, the interdigitated

method of two-finger has better performance than one-finger, and the three-finger are

still superior than two-finger.

From the n-type devices, it could be observed that the mean values of $\triangle$Vth and

$\triangle$Mu keep near to zero very closely and almost have no tendency.

For comparison, the case of p-type device in standard deviations of $\triangle$Vth and $\triangle$Muo are still examined as shown in Fig. 3-2-4. and Fig. 3-2-5. The standard deviations of the original and interdigitated devices are 0.028V, 0.020V, 0.016V for $\triangle$Vth and 1.704 cm^2/V*s, 1.178 cm^2/V*s, 0.958 cm^2/V*s for $\triangle$Mu, which reveal the similar properties as those of n-type devices. For both $\triangle$Vth and $\triangle$Mu in n-type and p-type devices, standard deviations decrease as finger number increases. However, the decreasing tendency seems to be smoother when the finger number increases. In order to investigate the trend, the reduction of mismatch with more fingers would be desired.

The deviation of $\triangle$Vth on both n-type and p-type devices for Poly-GroupA and Poly-GroupB, in each finger-number group, are shown in Fig 3-3-7 (a) and (b). In addition, the deviation of $\triangle$Mu on both n-type and p-type devices for Poly-GroupA and Poly-GroupB, in each finger-number group, are shown in Fig 3-3-8 (a) and (b). These figures clearly show that as the finger number increase, the standard deviation of device parameter differences decreases both in n-type and p-type for Poly-GroupA and Poly-GroupB devices. Table3-1 and Table3-2 list the standard deviation values for $\triangle$Vth and $\triangle$Mu for n-type and p-type devices, respectively. It is clear that the micro variation of devices can be suppressed by adopting the interdigitated layout and the more devices in the pair, the smaller micro variation of the pair would contain.

Concerning $\triangle$Vth in Fig 3-3-7 (a) and (b), it is noticeable that the standard deviation is inversely proportional to finger number. The $\triangle$Vth of p-type devices reveals the similar characteristics as shown in Fig. 3-3-7 (b). Since the standard deviations of $\triangle$Vth have the apparent properties of inverse proportionality with finger numbers, a proposed model would be desired to predict the performance :

$$y = a + bx^c \tag{3-1}$$

the values of certain parameters (a, b, c, R square) are shown in Table3-3.

In this place, the fitness of the model is compared with the coefficient of determination (R square). The square of the correlation coefficient (R square) presenting the fitness from the chosen equation will be used. R square is defined as:

$$r^2 = \frac{SSR}{SST} = 1 - \frac{SSE}{SST} \quad , \text{ where} \tag{3-2}$$

$$SSR = \sum (\hat{y} - \bar{y})^2 = \sum \hat{Y}^2 = b_1^2 \sum X_1^2 + b_2^2 \sum X_2^2 + 2b_1 b_2 \sum X_1 X_2$$

$$SST = \sum (y - \bar{y})^2$$

$$SSE = \sum \hat{e}^2 = \sum (y_i - \hat{y}_i)^2$$

R square indicates the similarity between the proposed model and the real data, and its value ranges between 0 and 1 [22]. It represents the proposed model can well model the data when R square value much approaches to 1. As shown in Table3-4, the values of R square are 0.9996 and 0.9988 for n-type and p-type devices, which is evident that the models presented are able to fit the data accurately. However, the predictive models have clearly indicated that there is practical limit to finger numbers as far as the enhancement of matching accuracy is concerned. As shown in Fig. 3-3-7 and Fig. 3-3-8, the predictive models for the standard deviation of △Vth and △Muo have nonzero intercept. Concerning the interdigitated devices of more fingers, only minute local process variations, and not global variations, affect them since they are within the same region. As finger number increases the local variation is uniformly spread and the devices are affected equally, thus the mismatch effect decreases.

The interdigitated methods with different number of fingers, distances and configurations are demonstrated. It can be well applied to describe the micro variation behaviors for poly silicon devices. The interest about the interdigitated method

18

applied to the single crystal silicon and the amorphous silicon devices is arisen. We will discuss this issue in the following section.

3-3 Other Devices with Different Grain Structures

In this section, we are interesting in the micro variation of the other devices with different grain structures, like the single crystal silicon and the amorphous silicon devices. More than 400 crosstie devices of amorphous silicon are measured and interdigitated statistically. The data of the single crystal silicon is referenced from Chee Lin Yum in Bachelor's thesis on Electrical Engineering [23]. The Fig. 3-3-1. shows the data of interdigitated method on ΔVth of n-type for a-Si, Poly-GroupA, Poly-GroupB, and c-Si devices, and those for the p-type are shown in Fig. 3-3-2. From these figures, we could clearly indicate that the proposed model is suitable for different grain structures. Table3-4 lists the fitting parameter of ΔVth with finger numbers for n-type different devices. Apart from amorphous silicon, the R square of poly silicon and single crystal silicon approach up to 0.98, it indicates that the good fitness between the proposed model and the real data. For the parameter "b" of equation (3-1), we find that the micro variation on ΔVth of poly silicon is ten times larger than single crystal silicon. Furthermore, the micro variation of amorphous silicon is three times larger than poly silicon. Table3-5 shows the fitting parameter of ΔVth with finger numbers for n-type different devices. For analyzing of the value "b" on p-type, we get the micro variation on ΔVth of poly silicon is one hundred times larger than single crystal silicon.

The Fig. 3-3-3 shows the data of interdigitated method on Δbeta of n-type for a-Si, poly-Si, and c-Si devices, and those for the p-type are shown in Fig. 3-3-4. Since we don't know the transistor's dimension and the oxide thickness from Yum's thesis, we can not compare the micro variation between each other. Table 3-6 and Table 3-7

show the fitting parameter of $\triangle$beta with device size (finger number) for n-type and p-type different devices respectively. The R square values are up to 0.99, indicating the tendency of the curve is the same and the high fitness of the proposed equation.

We successfully use the proposed model to describe the micro variation for different grain structures. With interdigitated method, as the finger number increases, the distributions of $\triangle$Vth and $\triangle$Mu are more concentrated and the variation range decrease. The tendency is similar to MOSFET's mismatch, where c=-0.5. And the micro variation of $\triangle$Vth in amorphous silicon is much larger than single crystal silicon and poly silicon. Therefore, we find that the micro variation of devices declines while device performance gets better.

The above results tell us that the larger channel width the devices have, the smaller the micro variation there will be. However, what the micro variation of the smaller channel width devices will be? Besides, since experimental data are not available for us to evaluate the micro variation behaviors for the smaller channel width device of the interdigitated layout, in the next chapter, we will introduce the simulation to investigate other properties of the micro variation.

Chapter 4

Mismatch Analysis Based on Simulation

4-1 Simulation Concept and Method

Since experimental data are not available for us to evaluate the micro variation behaviors for the smaller channel width device of the interdigitated layout, in this chapter, we will introduce the simulation to investigate other properties of the micro variation. In the beginning, we will briefly describe for the concept of the simulation. Fig. 4-1 shows the R square value on right vertical axis and standard deviation on left vertical axis with respect to the device size for Vth mismatch of the experimental data. The R square value is obtained by using the Gaussian distribution to fit the profile of the parameters difference. We classify this diagram into three regions, region I, region II and region III, by the yellow dotted lines. They will be discussed individually in the followings. We will discuss the region I in section 4-2, and region II and region III will be discussed later in section 4-3.

Before the simulation, it is essential to introduce the method of our simulation briefly. First, we integrate the assumed distribution of the parameters difference and its cumulative probability would be range from 0 ~ 100%. Second, we will transform this distribution into the corresponding value for Hspice simulation. For example, the Fig. 4-2 is a simple distribution with four variables. The random values from 0 ~ 1 are uniformly generated by computer and the transformed values can be obtained according to the Fig. 4-3. If we get 0.3 from computer, the variable B will be chosen according to Fig. 4-3. In the light of statistics theory, a certain number of data for each distribution will be generated in order to get the stable and reliable simulation result.

Fig. 4-4 shows the selected raw data and the two methods of simulation process, Method A and Method B. If the selected data are directly calculated in statistics, it is named "Method B". On the other hand, the Method A is applies the raw data to Hsipce to simulate the total current of the device in parallel. Then, the device parameters are extracted to calculate the mismatch. We will respectively examine the micro variation simulated by Method A and Method B.

Next section, we will simulate the different ranges of the parameters difference and try to investigate the correlation between the micro variation and different grain structure.

4-2 Simulation for the Profile of Mismatch with Different Ranges

Firstly, the problem we have to discuss is the region I that could be done by using the different ranges to evaluate the mismatching effect. From the results of the experimental data for a-Si, poly-Si, c-Si, we see that the mismatch will parallel shift in Y-axis and this difference may come from the different grain structures. Fig. 4-5 shows the Gaussian distribution with different ranges, $\gamma = 2$ and $\gamma = 4$, where parameter "γ" stands for the standard deviation. This figure shows that the standard deviation will affect the range of the profile. The smaller the parameter "γ" is, the smaller range the curve would have. Fig. 4-6 shows the different ranges of Gaussian distribution that was used to simulate the mismatch of Vth. The black, red and green lines respectively represent the standard deviation $\gamma = 1$, $\gamma = 3$ and $\gamma = 9$. The fitting parameters are listed in Table 4-1. It can be seen that the R square value is close to 1, which indicates the proposed model in equation (3-1) is still valid. The three lines just exhibit parallel shift on Y-axis, and it might have some correlation between the parameter "γ" of the Gaussian distribution equation and the fitting parameter "b" of the equation (3-1). The result of this diagram tells us that the range of the profile is the

dominant factor for the mismatch of the device. We find that the mismatch of device declines while standard deviation of the profile gets smaller. What is true for Vth mismatching simulation is true for Mu mismatching simulation as well. A similar result for Mu mismatch effect is shown in Fig. 4-7, and the fitting parameters are listed in Table 4-2. The tendency of Mu is the same as Vth that we mentioned above. What this section makes clear is that the behavior of the mismatch will parallel shift in Y-axis for different ranges, and this difference may correspond to different grain structures.

Next section, we will continue to discuss the region **II** in order to investigate the mismatching behavior of devices with smaller channel width.

4-3 Simulation for the Mismatch with Different Distributions

4-3-1 Mismatch of the devices with small channel width

We are interested in the mismatch of the smaller channel width since the smaller circuit layout area is preferred. So we want to discuss the region II of Fig. 4-1 in this section. The simulation will be done by using the different distributions to profile the parameters difference. First, we introduce the four distributions, Gaussian, Lorentzian, Gauss-Lorentzian and Uniform distribution, as shown in Fig. 4-8. Table 4-3 lists the equations and parameters for these different distributions.

Before the simulation, it is essential to introduce the inter-quartile range of the parameters difference. It is a major factor to decide the profile of these distributions. The inter-quartile range is the difference between the third and first quartiles of the data set, and including the variability of the middle 50 percent of the observations in the array. We take the same inter-quartile range of parameters difference for different distributions to simulate the mismatch effect here.

Fig. 4-9 shows the R square value on right vertical axis and standard deviation

on left vertical axis with respect to the device size for Vth mismatch calculated by Method A and B, respectively. As shown in the figure, the R square value of the Uniform distribution is below 0.9 in one-finger and two-finger, but it increases to 0.9 when the finger number is above three. This situation also happens in Lorentzian distribution for Method B. The result clearly shows that the distribution may possibly deviate from the Gaussian for the smaller channel width, according to the larger R square value. We also find that the profile of the parameters difference will resemble to Gaussian as the channel width increase. Similar to Fig. 4-9, the mismatch effect on Mu is shown in Fig. 4-10. It exhibits the same tendency as ΔVth, especially for one-finger, the R square value of the Uniform distribution for Method B is 0.34 only. Therefore, we want to examine the statistical diagram of the Uniform distribution more carefully. Fig. 4-11 shows the statistical diagram of the Uniform distribution for Method B with one-finger, five-finger, ten-finger and fifty-finger. This graph tells us that the shape will be more and more close to Gaussian for higher-finger, number devices, but it will stray from the Gaussian as the channel width decrease.

These results lead us to the conclusion that we may not be capable of evaluating the deviation for the smaller channel width device according to the behavior of large width devices. If we assume the profile of the parameters difference but the profile deviates from the Gaussian for the small channel width, the false estimation will be made.

For the data of Method B, the parameter differences are obtained directly from algebra calculation based on the statistical and therefore they may lack the consideration of device fundamental basis. For this reason, if we don't know the real profile of the parameters difference, the simulation results can not represent the micro variation precisely. Next, another direction of this simulation will be performed to investigate the mismatch of the large size devices in the region III of Fig. 4-1.

4-3-2 Mismatch of the devices with large channel width

In order to evaluate the micro variation of larger channel width device, we discuss the region III in this section. As mentioned above, the profile of parameters difference will resemble to Gaussian and the micro variation will decrease as the finger numbers increasing. However, from the viewpoint of micro variation, whether it will endlessly descend or not? We compare the experimental data of one-finger to six-finger devices to the simulation results of Method A and Method B in Fig. 4-12. For the experimental data, we can use both the proposed model in equation (3-1) and the exponential law to fit these curves well. The R square values of the fitting parameters based on equation (3-1) and exponential laws for the experiment data, and Method A, and Method B list in Table 4-4. We can not find obvious difference from the R square values because they are all above 0.99 for both Vth and Mu. For this reason, we must add the device pair with very large channel width to find the most suitable model out. It is not practical to collect the statistical results with measurement data. Thus, the simulation result is used here. Fig. 4-13 shows the device pair up to sixty-four fingers, for which we adopt Gaussian distribution to simulate the mismatch effect of Vth. We respectively use the power law and exponential law to fit the extend region. The R square values of the power law and exponential law are 0.992 and 0.878, respectively. The power law has better fitness than exponential law. It gives us an indication that the equation (3-1) might be more proper to describe the dependence of the standard deviation on the channel width. Similar to Fig. 4-13, the effects on Mu is shown in Fig.4-14. We also use the two equations to fit this curve and find that the R square of power law is still higher than exponential law. In conclusion, we could predict the micro variation for the larger channel width device by the model (power law) we proposed.

4-4 Summary

In this chapter, we try to evaluate the quantitative relationships between the variation and channel width in the regions where experimental data are not applicable. The simulation results are examined. From the discussion of region I, we find that the mismatch will parallel shift in Y-axis for different ranges, and the difference may come from different grain structures. Then, the standard deviation will increase and the profile will probably deviate from the Gaussian for the small channel width device. So we may fail to evaluate the mismatch for the region II. Lastly, we find that the proposed model in equation (3-1) has good fitness than the exponential law for the larger channel width device. It is possible to be used to evaluate the variation of the larger channel width devices, but may not be capable of predicting the smaller channel width ones.
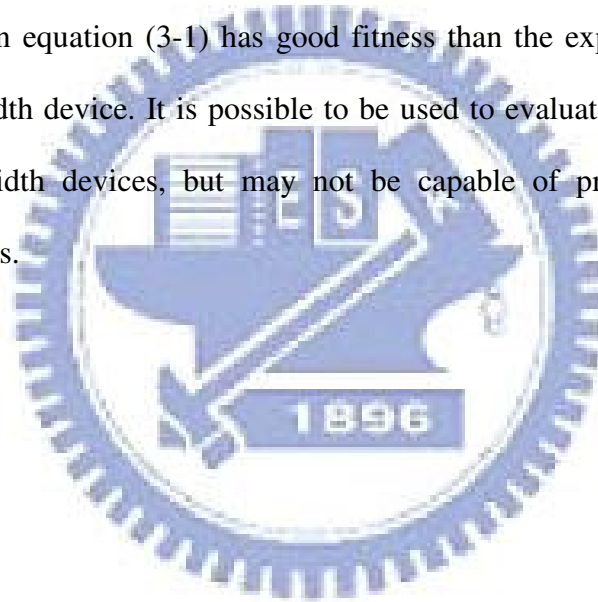
Chapter 5

Conclusion

In this thesis, the variation characteristics of LTPS TFTs are statistically investigated. In order to study the respective effects of micro and macro variation, a special layout of TFTs called "crosstie" is adopted in this work. By introducing this special layout of TFTs, the dependence of distance for device variations can be found. We classify two kinds of variation behaviors by grouping the difference of parameters in TFTs under different device distances. It can be observed that the variation in the range will be piecewise linear and the micro variation will be invariant in device position.

To further investigate the mismatching properties of the interdigitated arrangements, a huge number of devices with the same dimension are utilized. By analyzing the standard deviation of the parameters difference, it is found that the interdigitated method is indeed superior than the original one. Besides, threshold voltage and mobility are inversely proportional to the number of fingers, especially the threshold voltage. Therefore, a model of the micro variation is proposed to predict the performance of the interdigitated method, and it is proper to describe the variation behaviors with different device distances, for which the R square (Coefficient of Determinations) are higher than 0.98, which has high accuracy with the real data, reflecting the validity of the model. Besides, we applied the interdigitated method to the other devices with different grain structures, like the single crystal silicon and the amorphous silicon devices. For n-type devices, the micro variation of Vth in poly-Si is ten times larger than c-Si device, and the micro variation of Vth in a-Si is about three times larger than poly-Si device. The results tell us that the micro variations of

devices decline while device performance gets better. Furthermore, the proposed model is desired to evaluate the quantitative relationships between the variation and channel width in the regions where experimental data are not applicable. We find that the mismatch will parallel shift in Y-axis for different ranges, and the difference may come from different grain structures. Then, the standard deviation will increase and the profile will probably deviate from the Gaussian for the small channel width device. So we may fail to evaluate the mismatch for the region II. Lastly, we find that the proposed model in equation (3-1) has good fitness than the exponential law for the larger channel width device. It is possible to be used to evaluate the variation of the larger channel width devices, but may not be capable of predicting the smaller channel width ones.

In conclusion, in order to suppress the mismatch effect, the methods of interdigitated are concerned since the fabrication process is predetermined. From the view points of statistical analysis, contributions of interdigitated are demonstrated by parameter distributions of large amount of devices. In addition, we propose a model to evaluate the inverse proportionality of the interdigitated method, which could be used to predict the mismatch property of devices.

References

[1] Chun-Yen Liu, Kuo-Bin Hsu, Ryan Lee, Chang-Ho Tseng, Shin-Chang Chang, and Yaw-Ming Tsai, "High performance fully self-aligned symmetric LDD TFT for system-on-panel display," in *SID Tech. Dig.*, 2005, pp. 308-311.

[2] Kiyoshi Yoneda, Hidenori Ogata, Shinji Yuda, Kohji Suzuki, Toshifumi Yamaji, Shiro Nakanishi, Tsutomu Yamada, and Yoshihiro Morimoto, "Optimization of low-temperature poly-Si TFT-LCDs and a large-scale production line for large glass substrates," *Journal of the SID*, vol. 9, pp. 173-179, 2001.

[3] Y. Matsueda, T. Ozawa, M. Kimura, T. Itoh, K. Kitwada, T. Nakazawa, H. Ohsima, "A 6-bit-color VGA low-temperature poly-Si TFT-LCD with integrated digital data drivers," in *SID Tech. Dig.*, 1998, pp. 879-882.

[4] J. G. Blake, J. D. III Stevens, and R. Young, "Impact of low temperature polysilicon on the AMLCD market," *Solid State Tech.*, vol. 41, pp. 56-62, 1998.

[5] Y. Aoki, T. Lizuka, S. Sagi, M. Karube, T. Tsunashima, S. Ishizawa, K. Ando, H. Sakurai, T. Ejiri, T. Nakazono, M. Kobayashi, H. Sato, N. Ibaraki, M. Sasaki, and N. Harada, "A 10.4-in. XGA low-temperature poly-Si TFT-LCD for mobile PC applications," in *SID Tech. Dig.*, 1999, pp. 176-179.

[6] S. D. Brotherton, J. R. Ayres, M. J. Edwards, C. A. Fisher, C. Glaister, J. P. Gowers, D. J. McCulloch, and M. Trainor, "Laser crystallized poly-Si TFTs for AMLCDs," *Thin Solid Films*, vol. 337, pp. 188–195, 1999

[7] S. D. Brotherton, D. J. McCulloch, J. P. Gowers, J. R. Ayres, C. A. Fisher, and F. W. Rohlfing, "Excimer laser crystallization of poly-Si TFTs for AMLCDs," in *Proc. Mat. Res. Soc. Symp.*, vol. 621, 2000, pp. Q7.1.1–Q7.1.12.

[8] H. J. Kim, D. Kim, J. H. Lee, I. G. Kim, G. S. Moon, J. H. Huh, J. W. Hwang, S. Y. Joo, K. W. Kim, and J. H. Souk, "A 7-in. full-color low-temperature poly-Si

TFT-LCD," in *SID Tech. Dig.*, 1999, pp. 184-187.

[9] J. H. Jeon, M. C. Lee, K. C. Park, and M. K. Han, "A new polycrystalline silicon TFT with a single grain boundary in the channel," *IEEE Electron Device Lett.*, vol. 22, pp. 429-431, 2001.

[10] A. G. Lewis, T. Y. Huang, I. W. Wu, R. H. Bruce, and A. Chiang, "Physical mechanisms for short channel effects in polysilicon thin film transistors," in *IEDM Tech. Dig.*, 1989, pp. 349-352.

[11] Dimitrios N. Kouvatsos, Apostolos T. Voutsas, and Miltiadis K. Hatalis, "High-performance thin film transistors in large grain size polysilicon deposited by thermal decomposition of disilane," *IEEE Trans. Electron Devices*, vol. 43, pp. 1399-1406, 1996.

[12] Y. C. Wu, Y. C. Wu, C. W. Chou, C. H. Tu, J. C. Lou, C. Y. Chang, T. C. Chang, and P. T. Liu, "Mobility enhancement of pattern-dependent metal-induced lateral crystallization polysilicon thin-film transistors with different dimensions," in *SID Tech. Dig.*, 2005, pp. 268-271.

[13] S. Uchikoga and N. Ibaraki, "Low temperature poly-Si TFT-LCD by excimer laser anneal," *Thin Solid Films*, vol. 383, pp.19-24, 2001

[14] S. D. Brotherton, D. J. Mcculloch, J. B. Ciegg, and J. P. Gowers, "Excimer-laser-annealed poly-Si thin-film transistors," *IEEE Trans. Electron Devices*, vol. 40, pp. 407-413, 1993.

[15] Do-Hyun Choi, Eiichi Sadayuki, Osamu Sugiura, and Masakiyo Matsumura, "Lateral growth of poly-Si Film by excimer laser and its thin film transistor applications," *Jpn. J. Appl. Phys. Part1*, vol. 33, pp. 70-74, 1994.

[16] Kitahara, Yoshiyuki, Toriyama, Shuichi, Sano, Nobuyuki, "A new grain boundary model for drift-diffusion device simulations in polycrystalline silicon thin-film transistors", *Japanese Journal of Applied Physics, Part 2: Letters*, v

42, n 6 B, pp. L634-L636 (2003).

[17] Wang, Albert W. and Saraswat, Krishna C.," Modeling of grain size variation effects in polycrystalline thin film transistors" , *Technical Digest International Electron Devices Meeting*, pp. 277-280 (1998).

[18] Wang, Albert W. and Saraswat, Krishna C.," Strategy for modeling of variations due to grain size in polycrystalline thin-film transistors", *IEEE Transactions on Electron Devices*, v 47, n 5, pp. 1035-1043 (2000).

[19] M. J. M. Pelgrom, A. C. J. Duinmaijer, and A. P. G. Welbers," Matching properties of MOS transistors," *IEEE J. Solid State Circuits*, vol.**24**, pp.1433-1989, 1989.

[20] Shi-Zhe Huang," Statistical Study on the Uniformity Issue of Low Temperature Polycrystalline Silicon Thin Film Transistor", *Diss. National Chiao Tung University*, p. 14, 2005.

[21] N. Yamauchi, J-J. J. Hajjar, and R. Reif, "Polysilicon thin-film transistors with channel length and width comparable to or smaller than the grain size of the thin film," *IEEE Electron Devices*, vol.**38**, pp.55-60, 1991.

[22] Devore, "Applied Statistics for Engineers and Scientists", Thomson, Second Edition, 2005.

[23] Chee-Lin Yum," Statistical Evaluation of Layout Techniques and Device Size for Characterizing The Matching Behavior of N- and P- Channel Differential Pairs", *BSEE. University of Southern Maine*, 1996
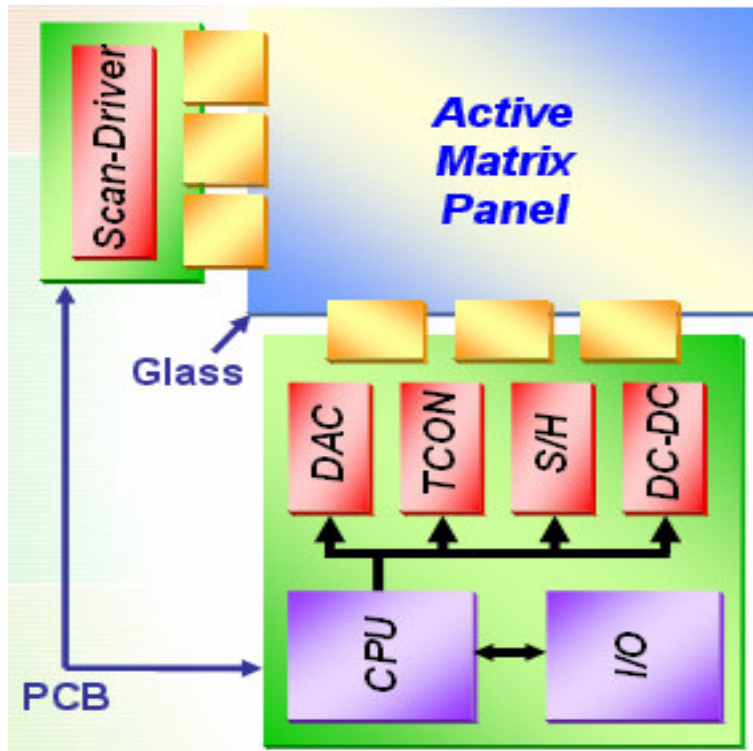
Fig. 1-1. The block diagram of an active matrix display
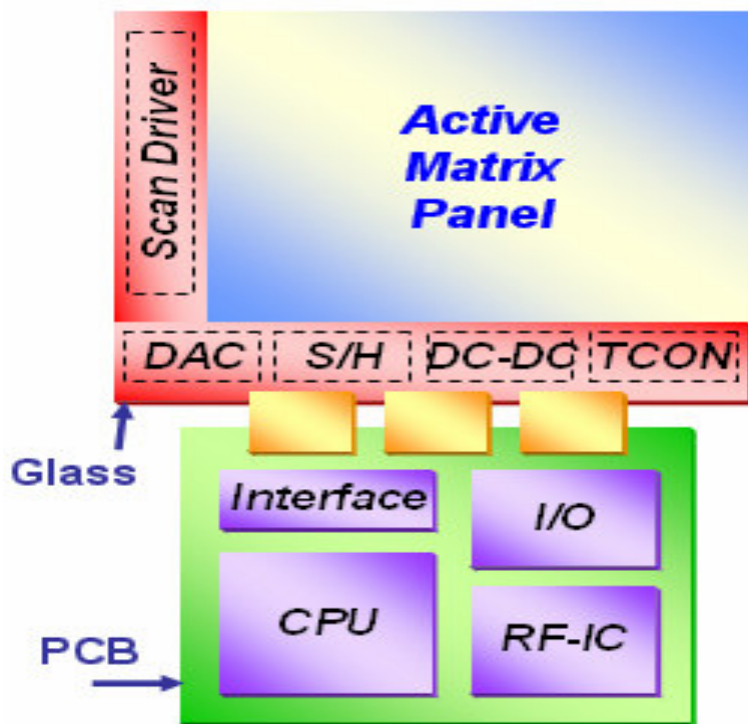
Fig. 1-2. The integration of peripheral circuits in a display achieved by poly-Si TFTs
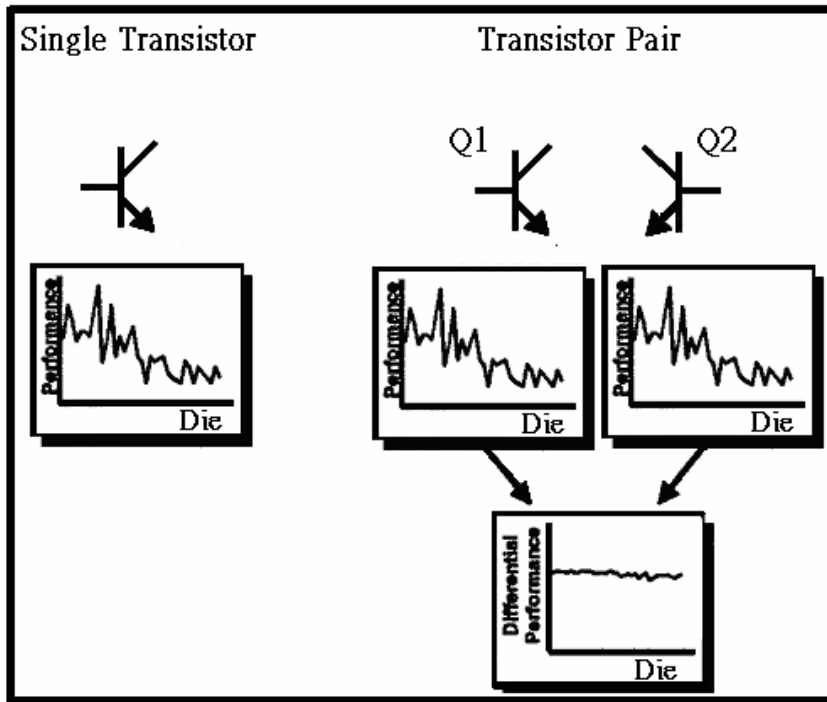
Fig. 1-3. The purpose of matching is to have circuit performance based on the differential performance of two devices rather than the absolute performance of a single device.

<div align="center">(a)   (b)</div>
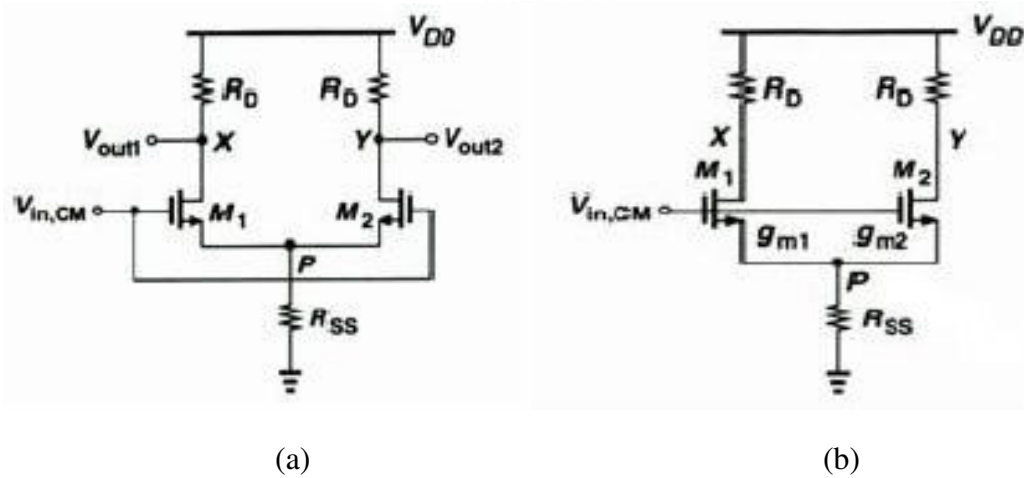
Fig. 1-4. Common-mode response in the presence of transistor mismatch (a) Differential pair sensing CM input. (b) equivalent circuit of (a)
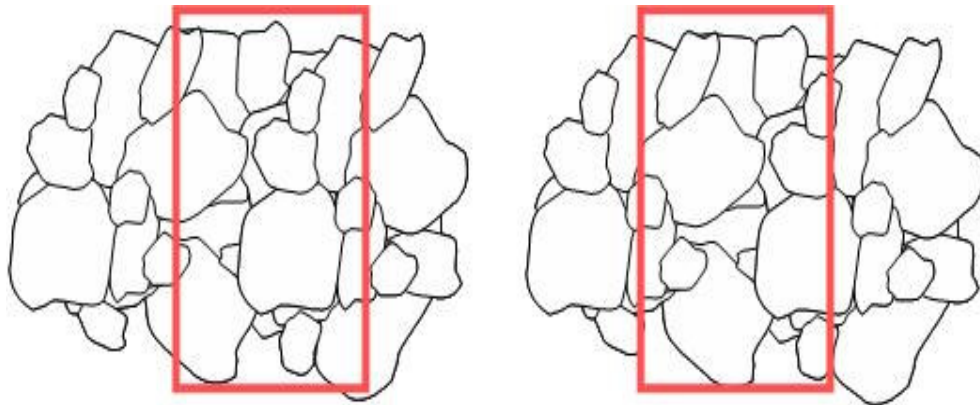
Fig. 1-5. The initial characteristics of LTPS TFTs are different from one another due to various distributions of grain boundaries
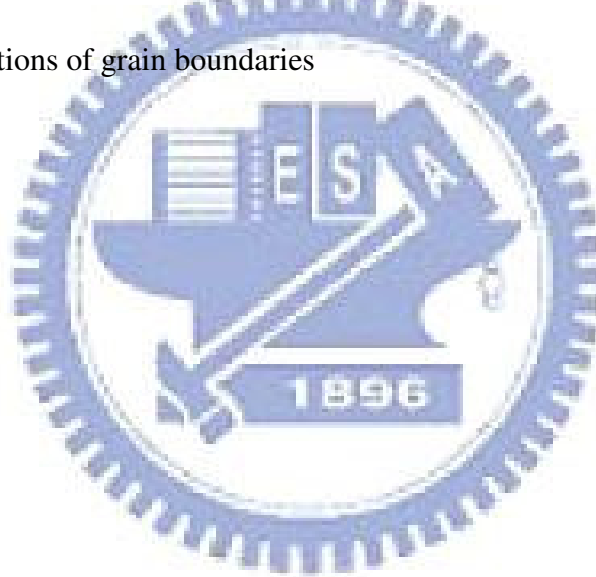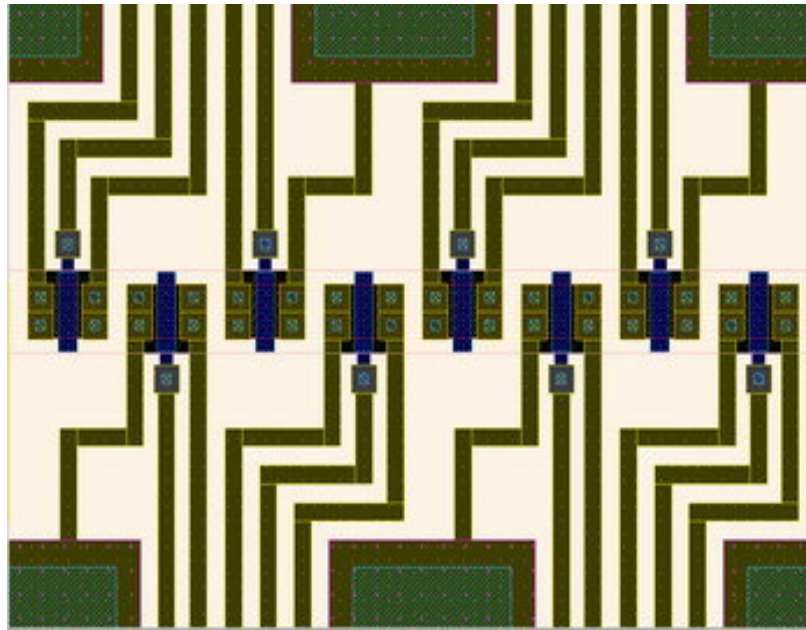
(a)
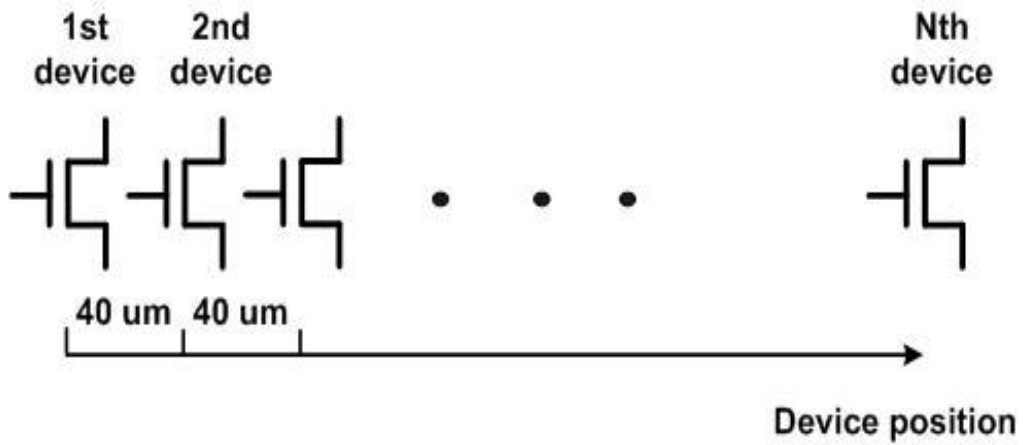
(b)

Fig. 2-1. (a)The layout of the crosstie TFTs. (b) The distance of two nearest active regions is equally-spaced 40µm
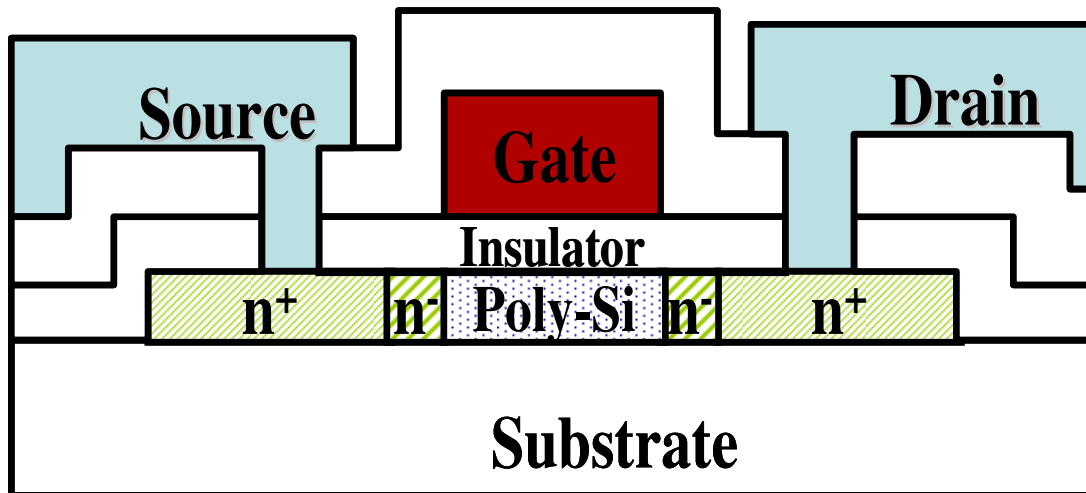
Fig. 2-2. The schematic cross-section structure of the n-type poly-Si TFT with lightly doped drain
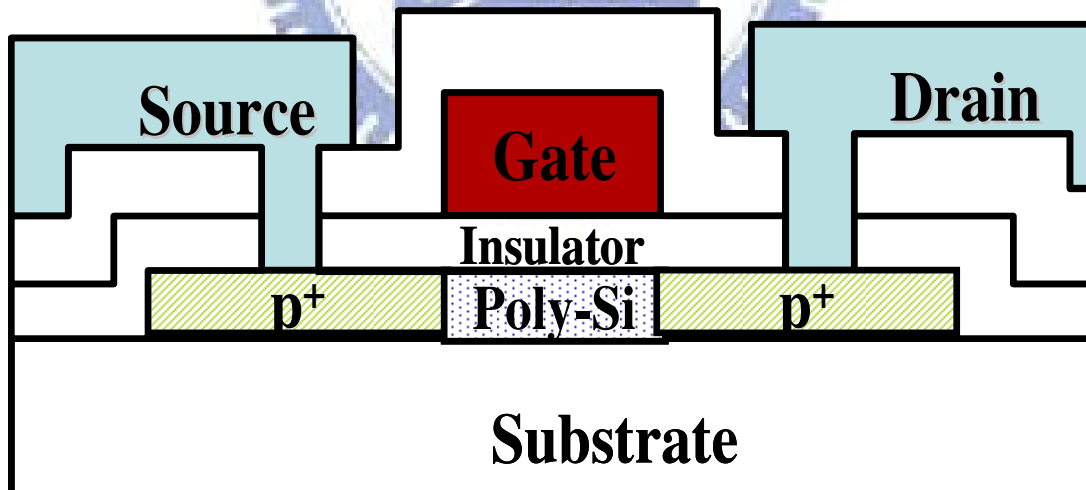
Fig. 2-3. The schematic cross-section structure of the p-type poly-Si TFT without lightly doped drain
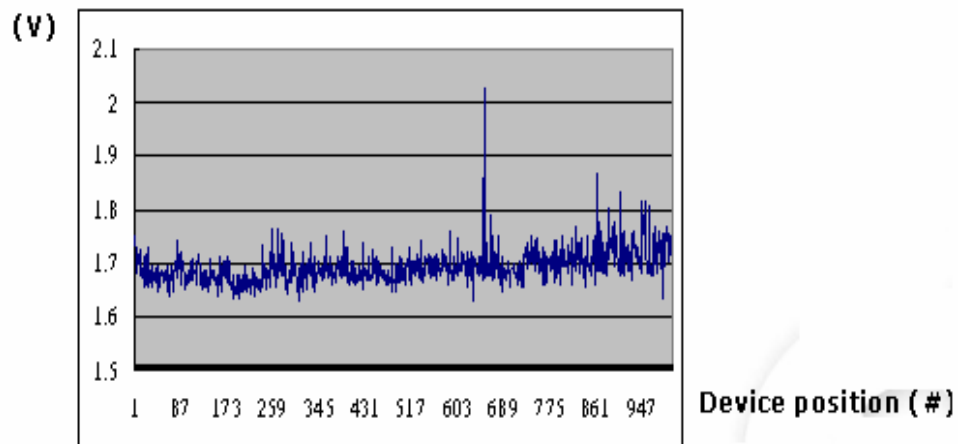
Fig. 3-1-1 The threshold voltage distribution along the device position
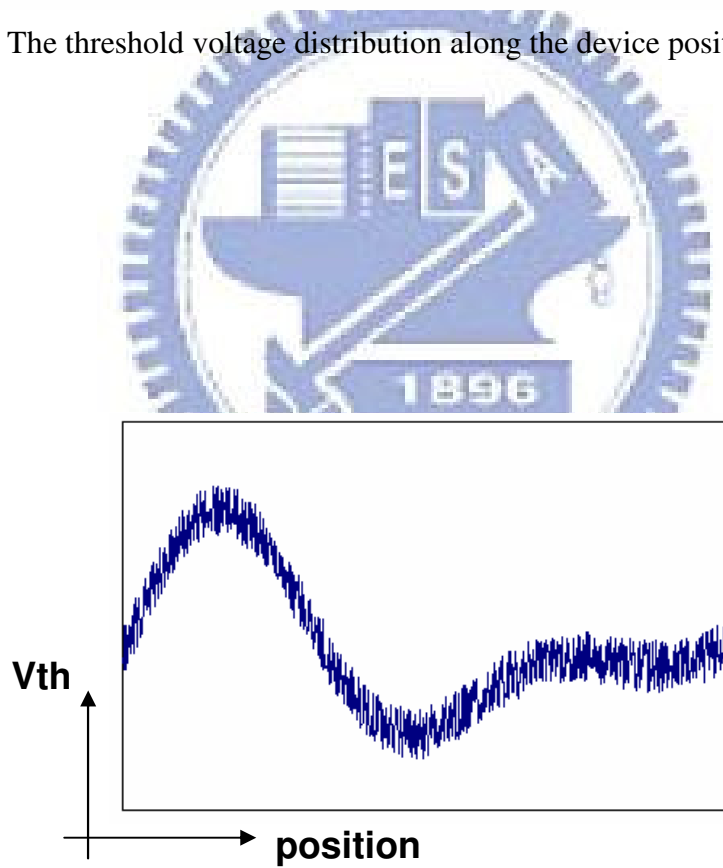
Fig. 3-1-2 Simulation of the threshold voltage distribution along the device position

for a long range

37
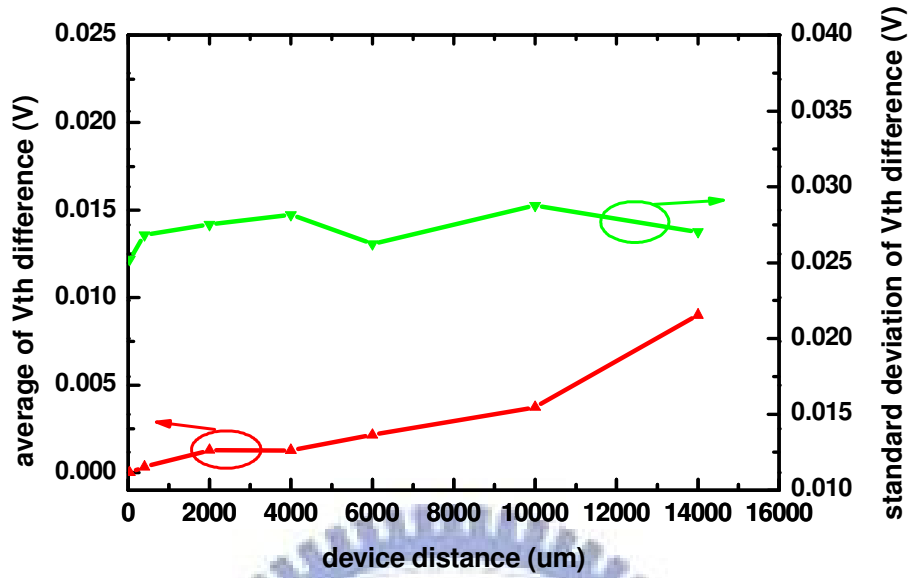
(a) N-type of Poly-GroupA devices
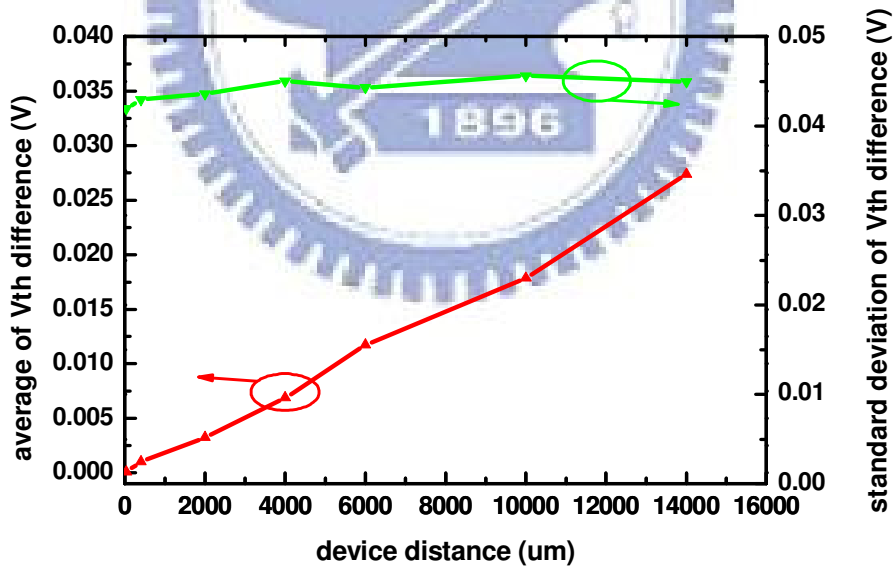
(b) N-type of Poly-GroupB devices

Fig. 3-1-3 The average and the standard deviation of the differences of threshold voltage of N-type devices (a) Poly-GroupA (b) Poly-GroupB
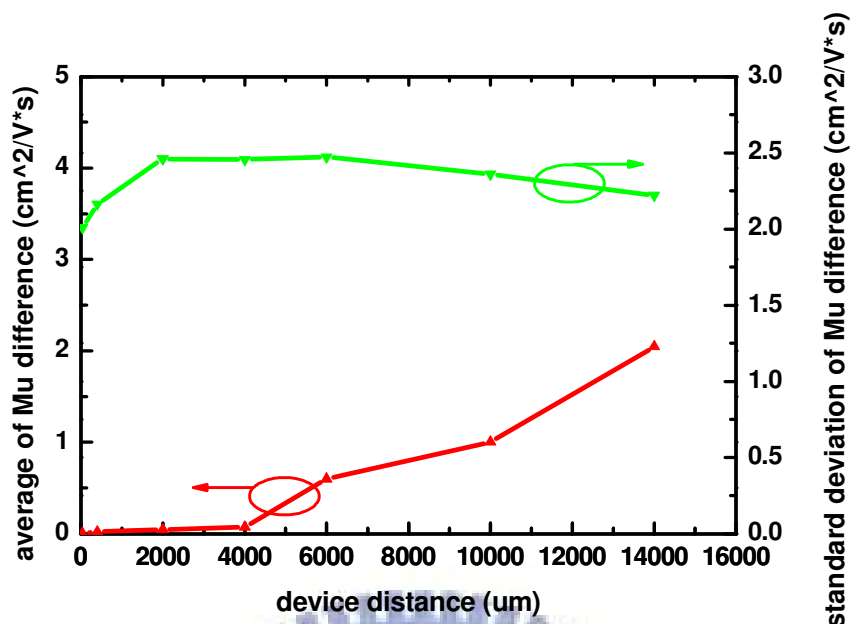
(a) N-type of Poly-GroupA devices
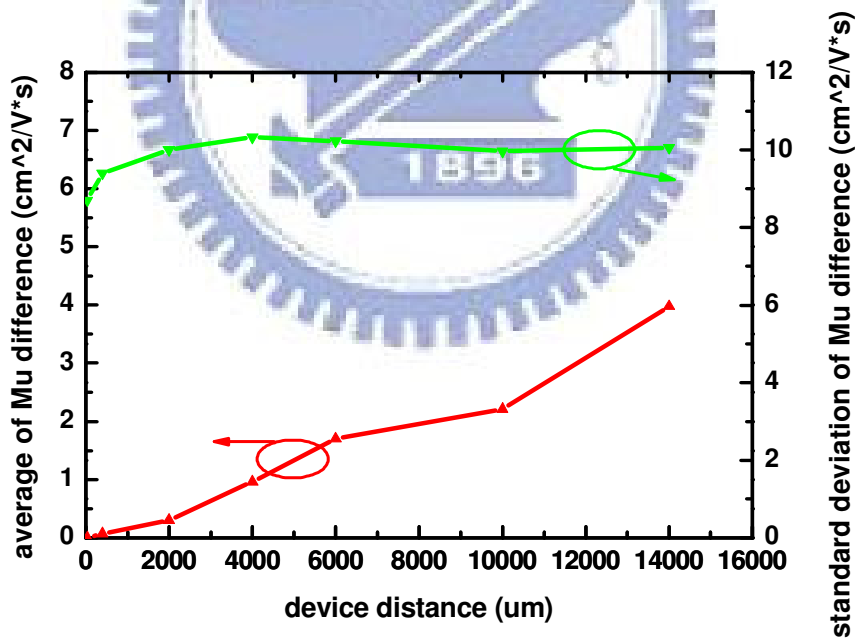
(b) N-type of Poly-GroupB devices

Fig. 3-1-4 The average and the standard deviation of the differences of mobility of N-type devices(a)Poly-GroupA (b)Poly-GroupB
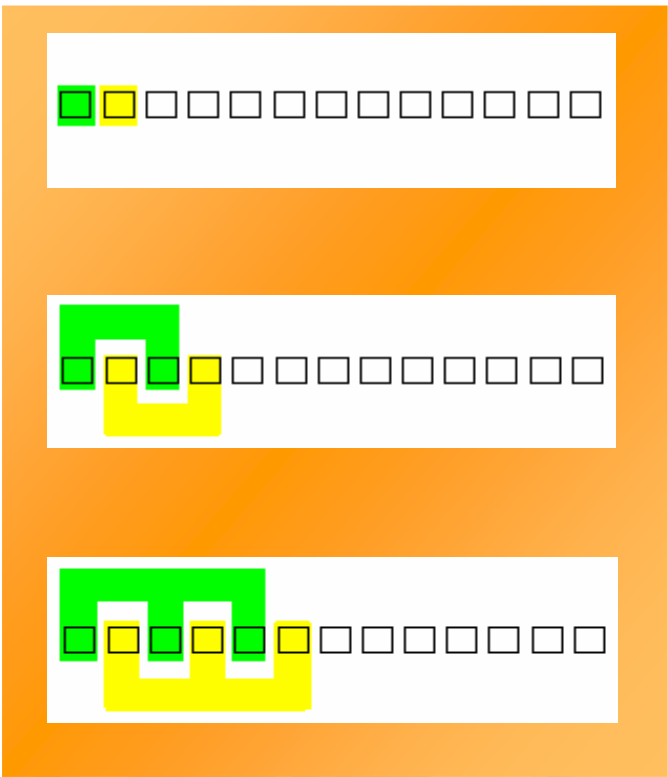
Fig. 3-2-1. Illustration of the interdigitated method of the crosstie device
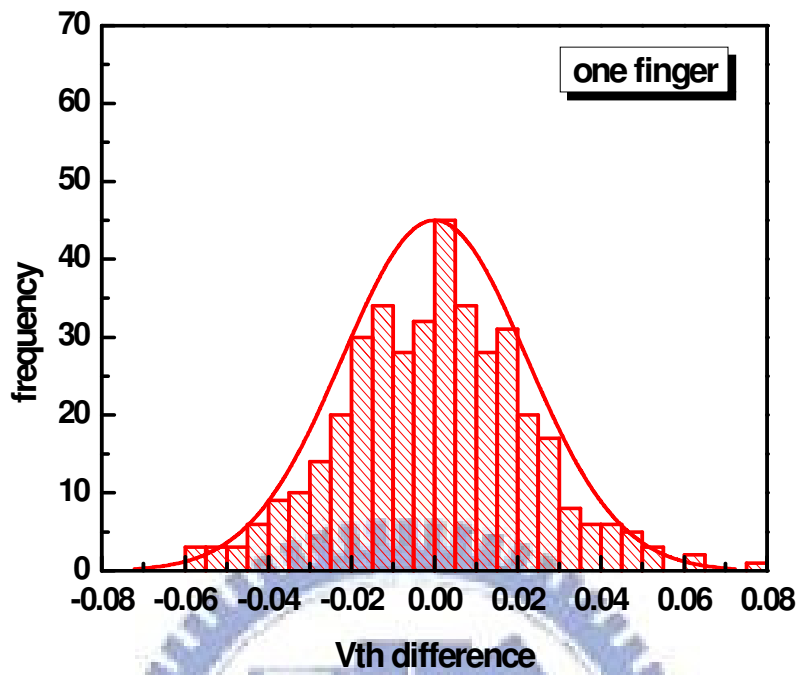
(a) interdigitated method of one-finger
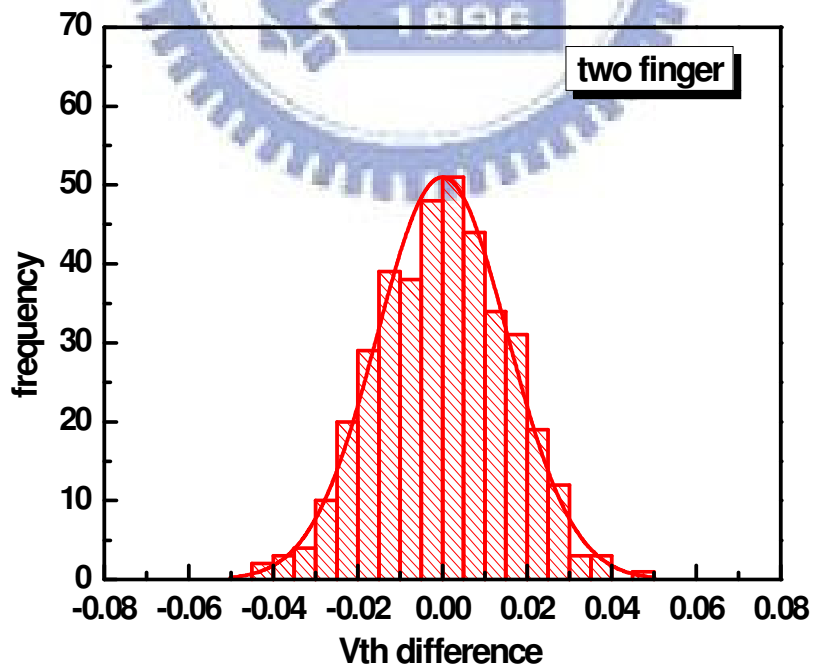
(b) interdigitated method of two-finger
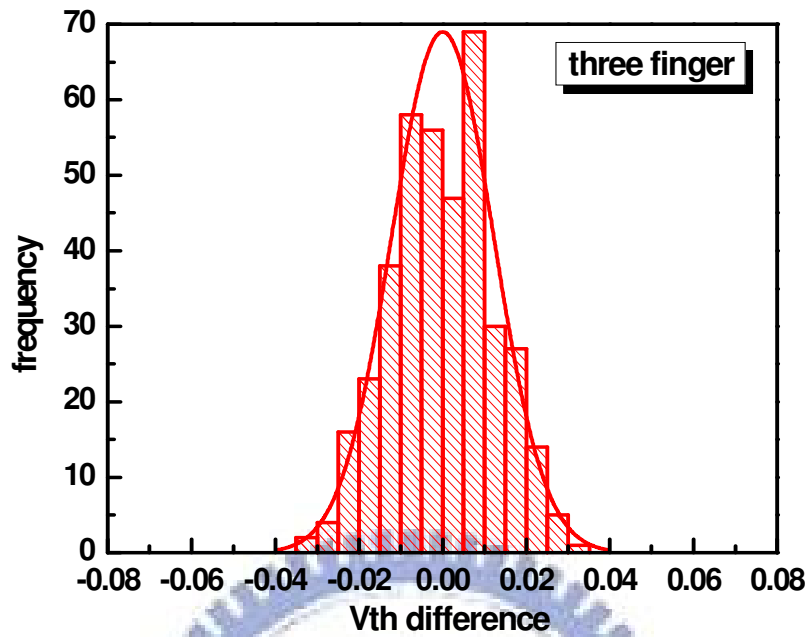
(c) interdigitated method of three-finger

Fig. 3-2-2 Poly-GroupA N-type device distributions of threshold voltage difference between original and the interdigitated methods (a) interdigitated method of one-finger (b) interdigitated method of two-finger (c) interdigitated method of three-finger
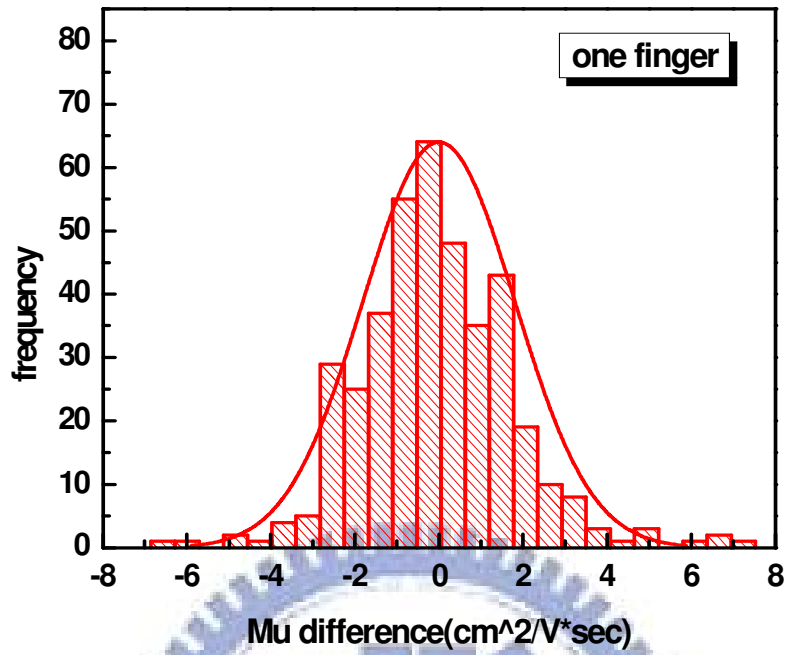
(a) interdigitated method of one-finger
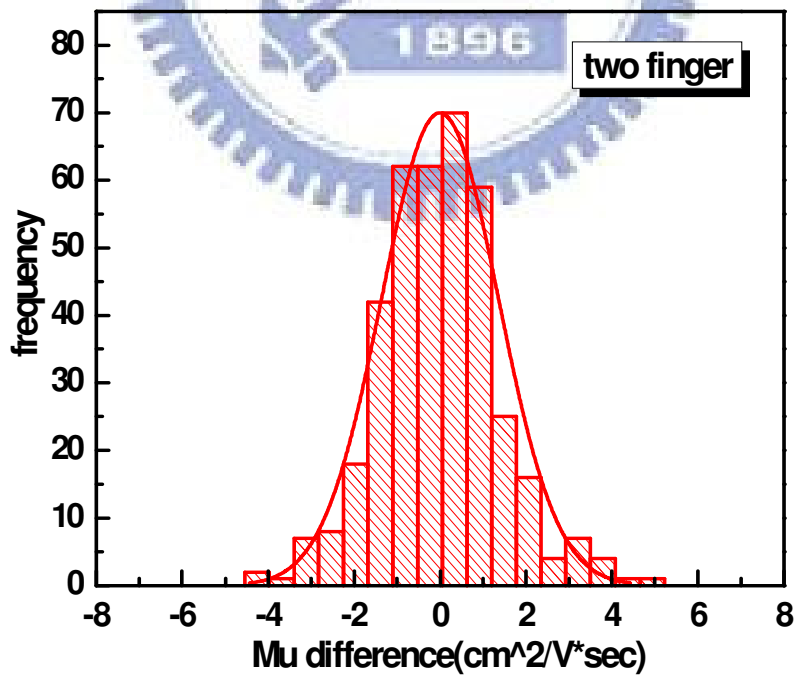
(b) interdigitated method of two-finger
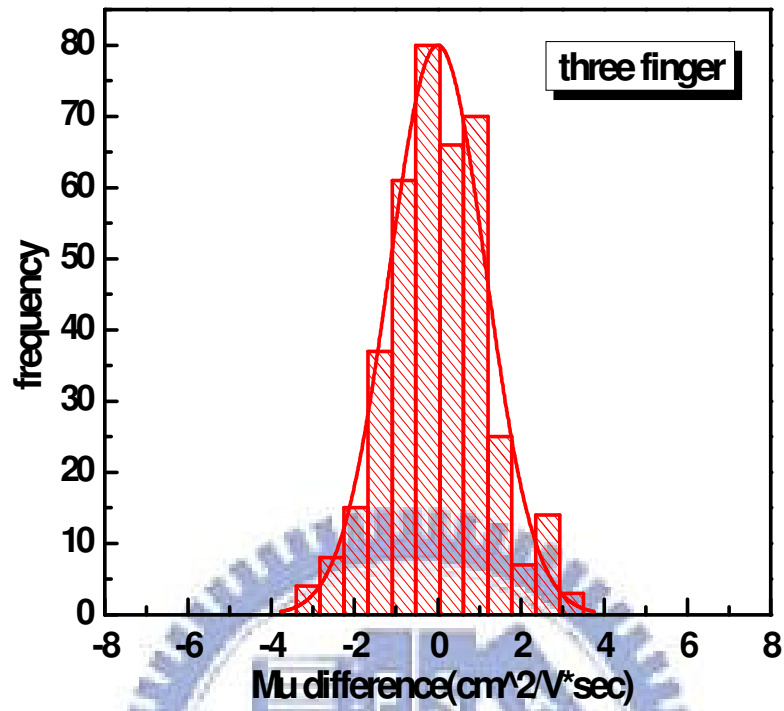
(c) interdigitated method of three-finger

Fig. 3-2-3 Poly-GroupA N-type device distributions of mobility difference between original and the interdigitated methods (a) interdigitated method of one-finger (b) interdigitated method of two-finger (c) interdigitated method of three-finger
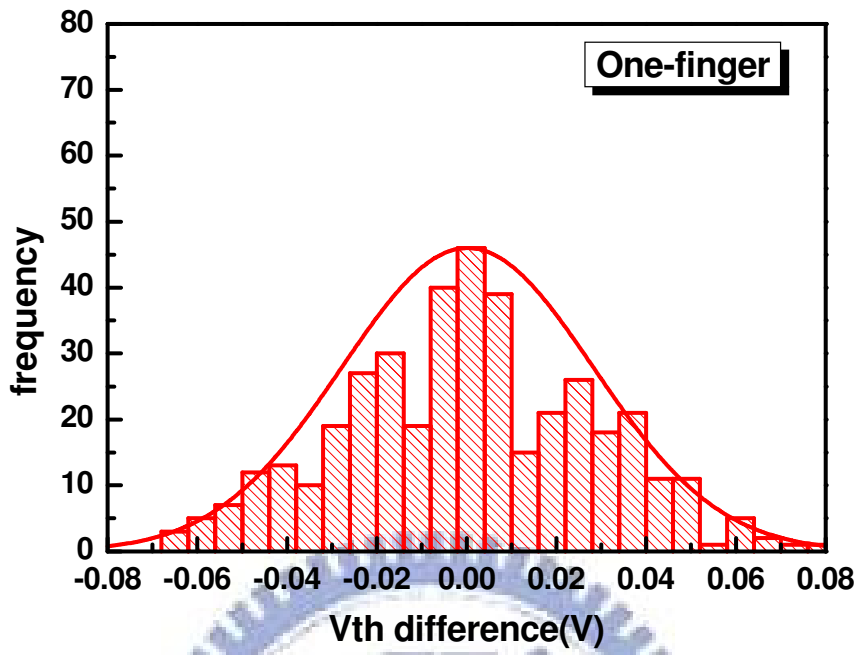
(a) interdigitated method of one-finger
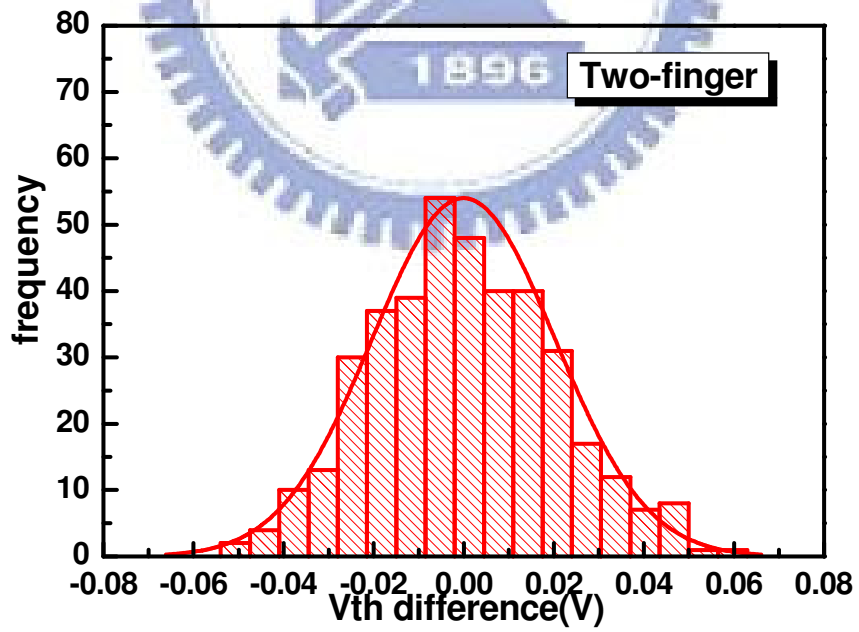
(b) interdigitated method of two-finger
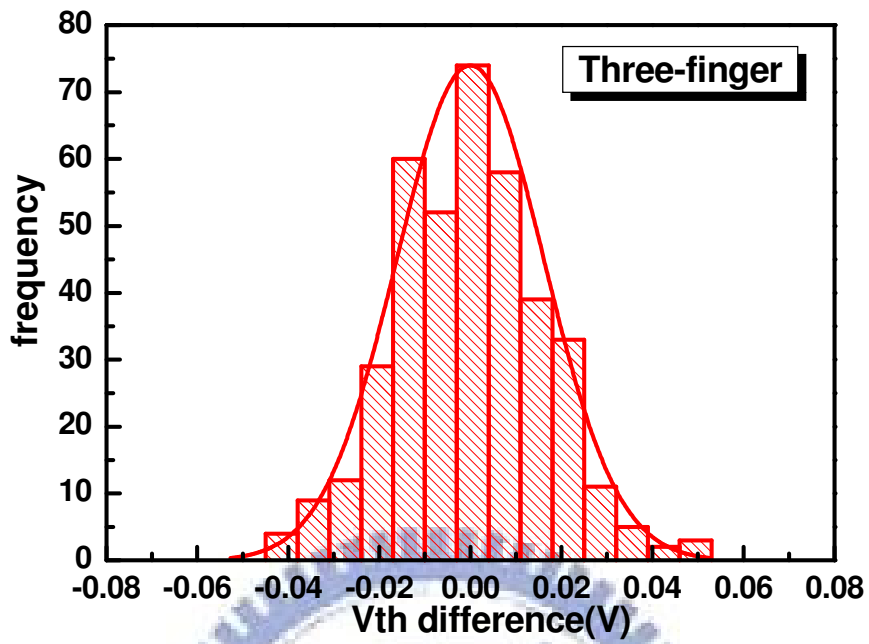
(c) interdigitated method of three-finger

Fig. 3-2-4 Poly-GroupA P-type device distributions of threshold voltage difference between original and the interdigitated methods (a) interdigitated method of one-finger (b) interdigitated method of two-finger (c) interdigitated method of three-finger
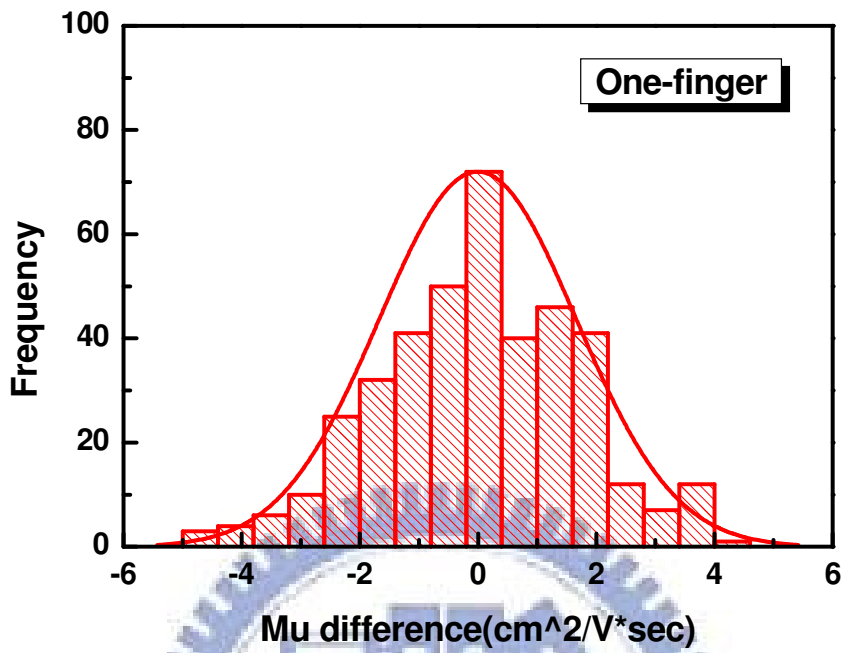
(a) interdigitated method of one-finger
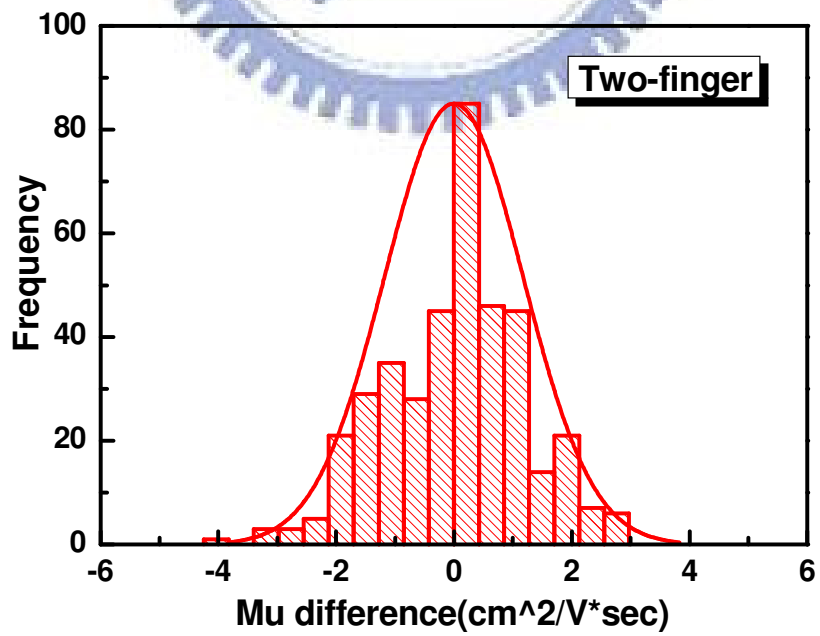
(b) interdigitated method of two-finger
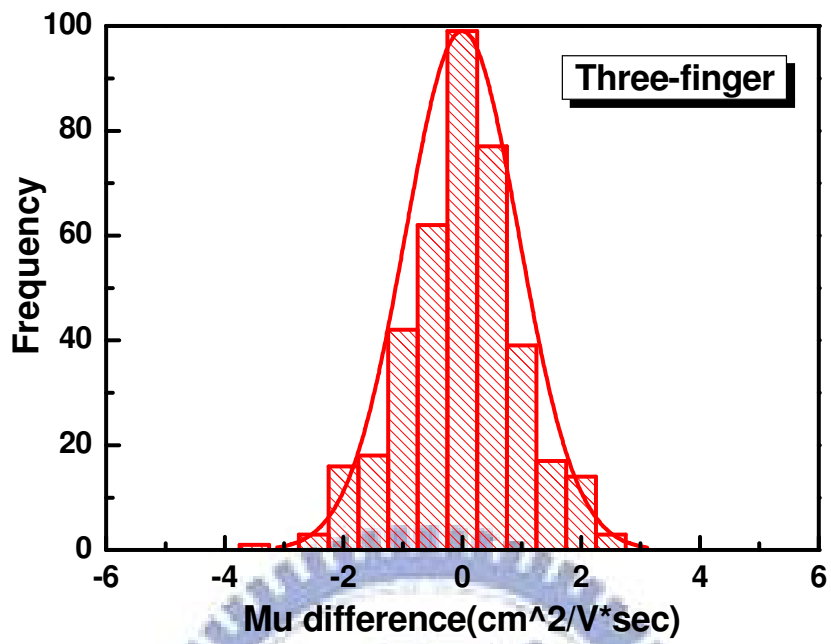
(c) interdigitated method of three-finger

Fig. 3-2-5 Poly-GroupA P-type device distributions of mobility difference between original and the interdigitated methods (a) interdigitated method of one-finger (b) interdigitated method of two-finger (c) interdigitated method of three-finger

Fig. 3-2-6. Illustration of the interdigitated method of the crosstie device with more fingers
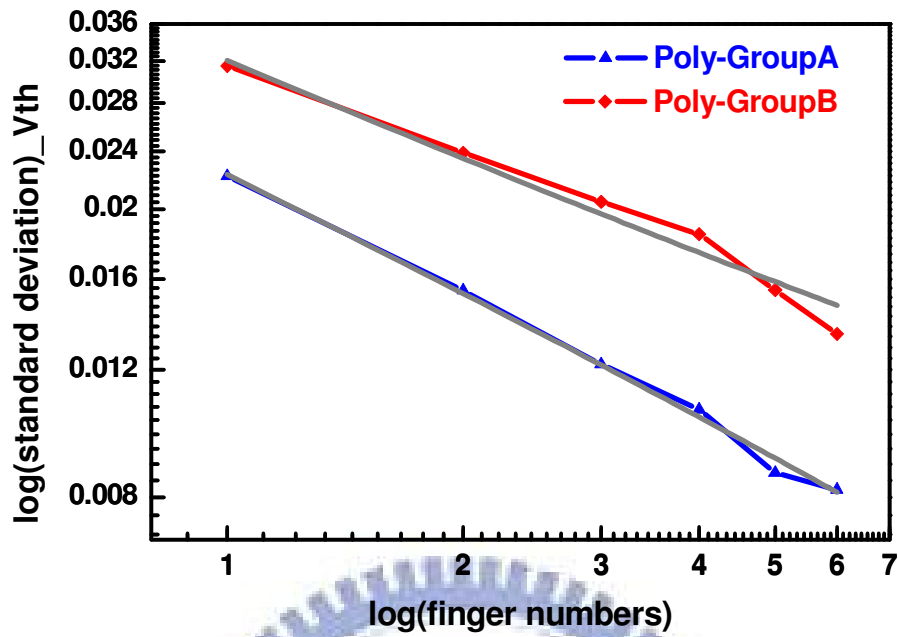
(a) n-type devices
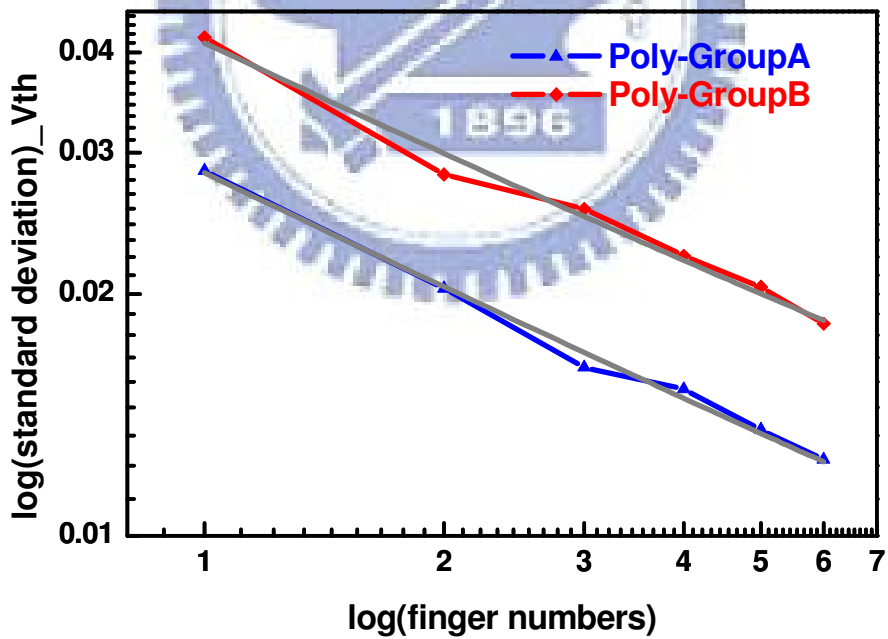
(b) p-type devices

Fig. 3-2-7. Measured data and model for devices with different channel width (a) △ Vth of n-type device (b) △Vth of p-type device
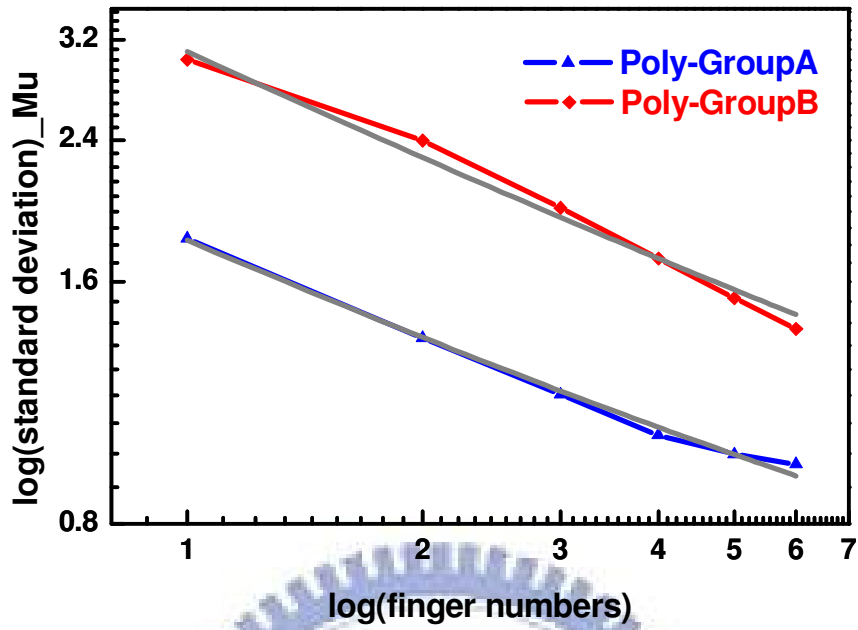
(a) n-type deives
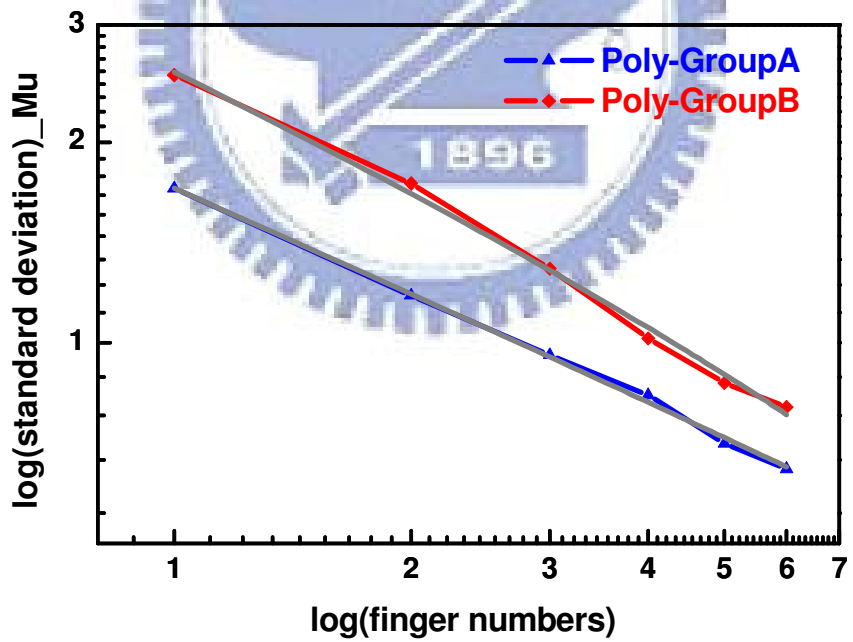
(b) p-type devices

Fig. 3-2-8. Measured data and model for devices with different channel width (a) △ Muo of n-type device (b) △Muo of p-type device.
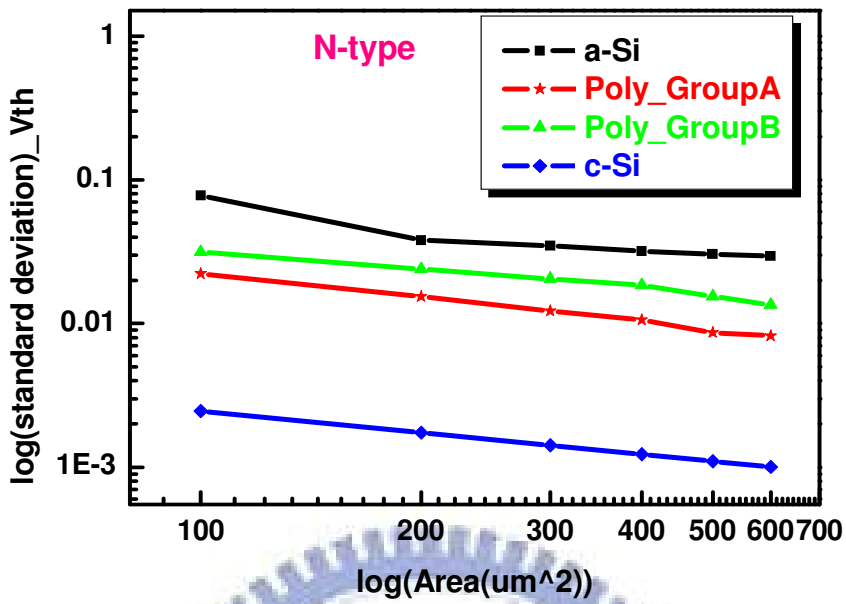
Fig 3-3-1 The data of interdigitated method on ΔVth of n-type for a-Si, poly-Si, and
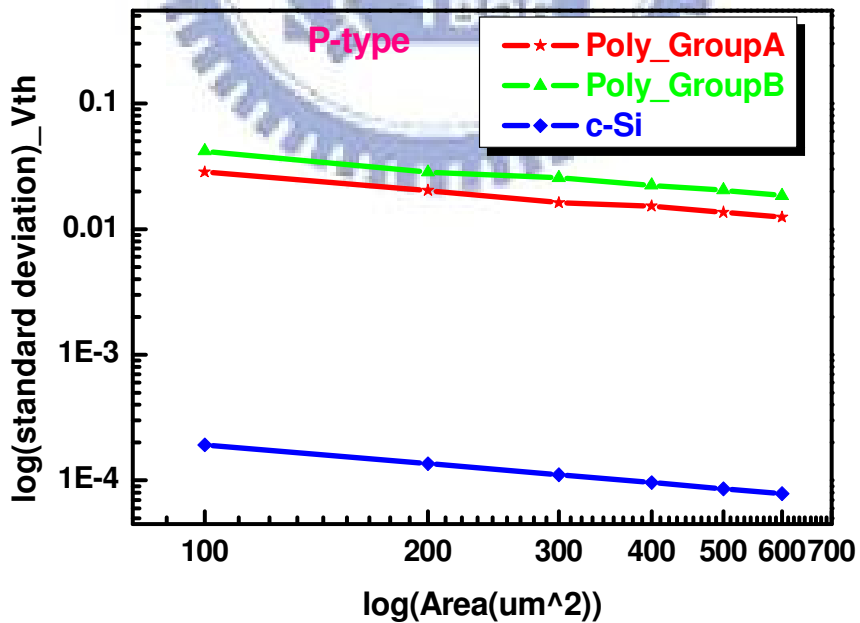
c-Si devices.

Fig.3-3-2 The data of interdigitated method on ΔVth of p-type for poly-Si, and c-Si

devices.
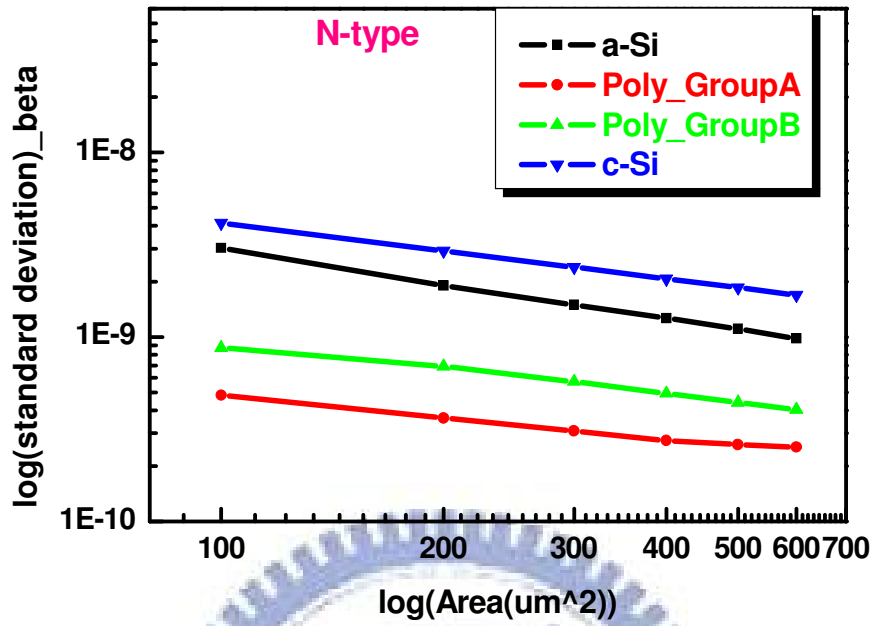
Fig.3-3-3 The data of interdigitated method on △beta of n-type for a-Si, poly-Si, and
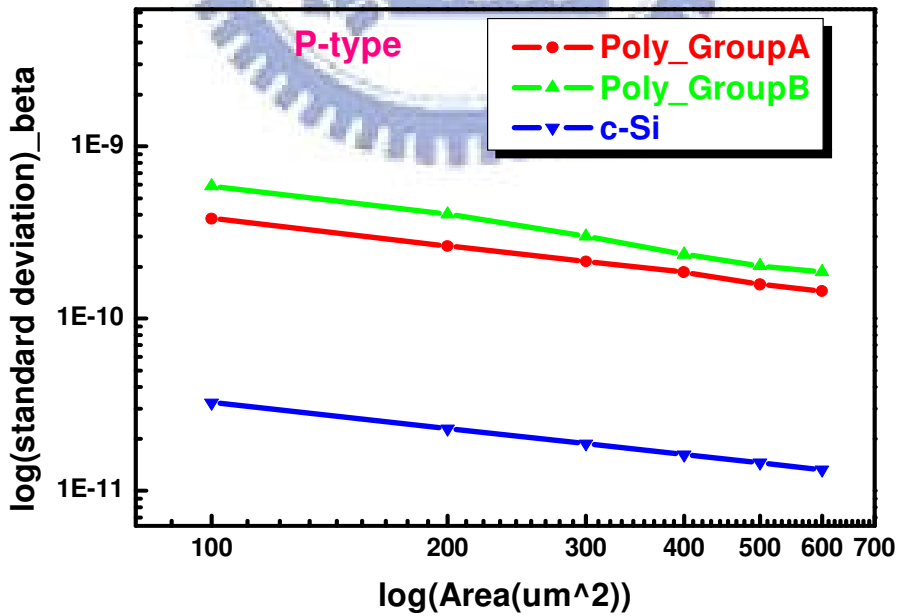
c-Si devices.

Fig.3-3-4 The data of interdigitated method on △beta of p-type for a-Si, poly-Si, and

c-Si devices.
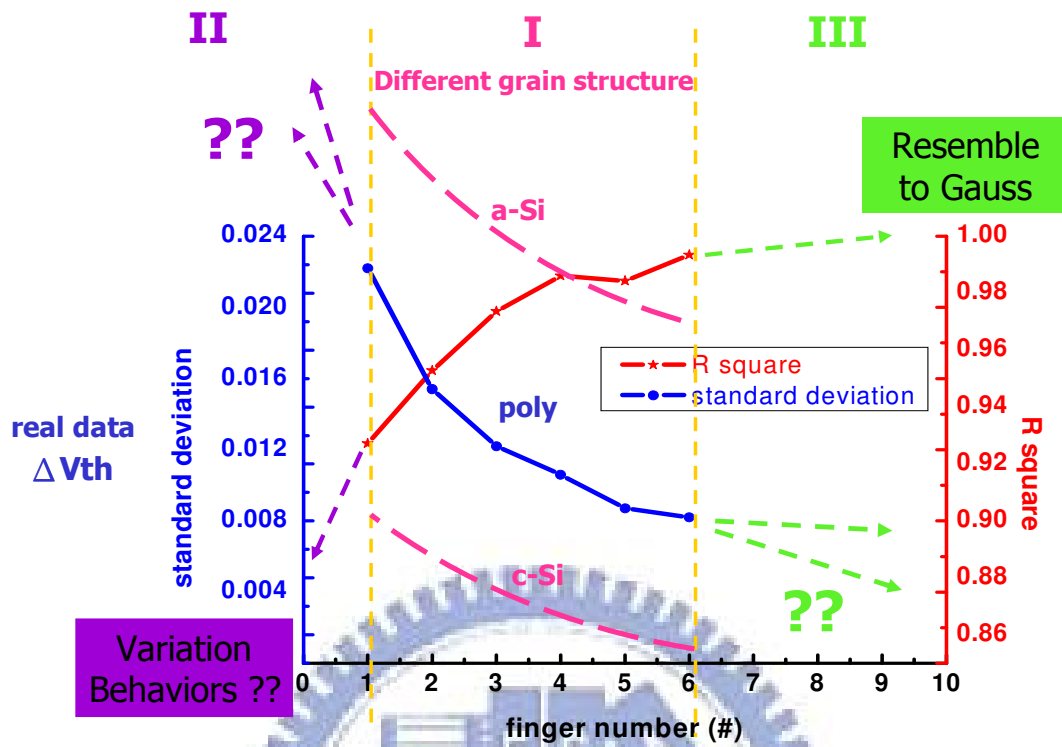
Fig 4-1 The R square value on right vertical axis and standard deviation on left vertical axis with respect to the device size for Vth mismatch of the experimental data. We classify this diagram into three regions, region I, region II and region III, by the yellow dotted lines.
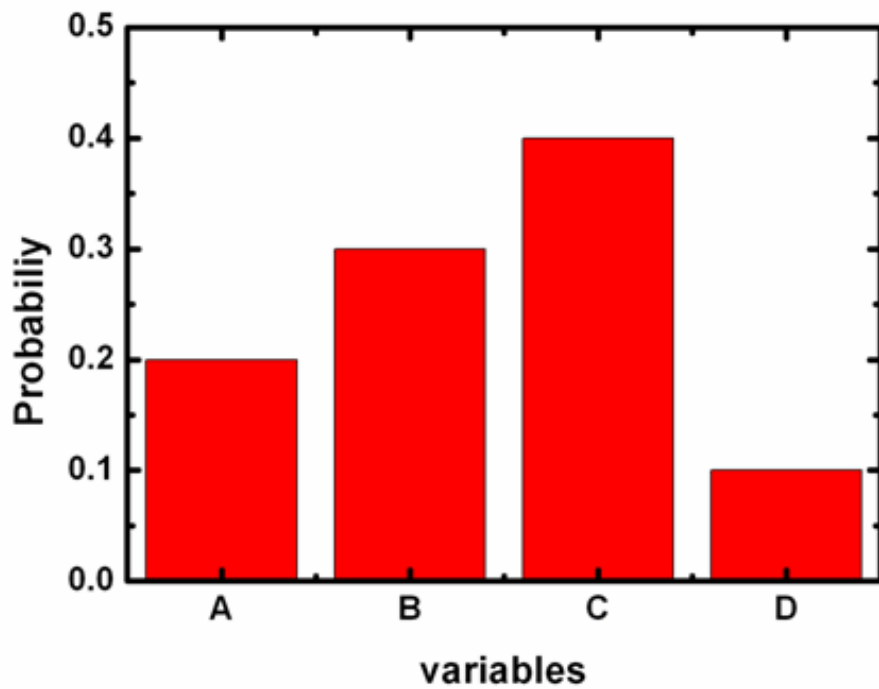
Fig. 4-2 Simple distribution with four variables.
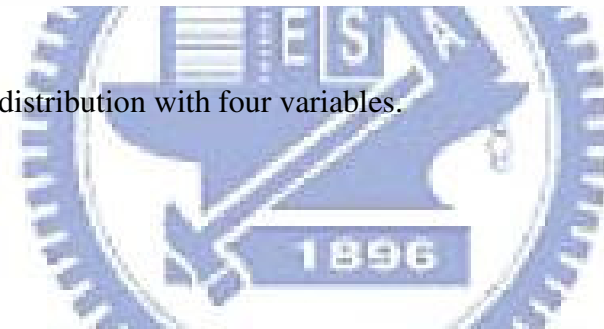
Random value	Corresponding variable
0 ~ 0.2	A
0.2 ~ 0.5	B
0.5 ~ 0.9	C
0.9 ~ 1.0	D

Fig. 4-3 The chart for data transformation.
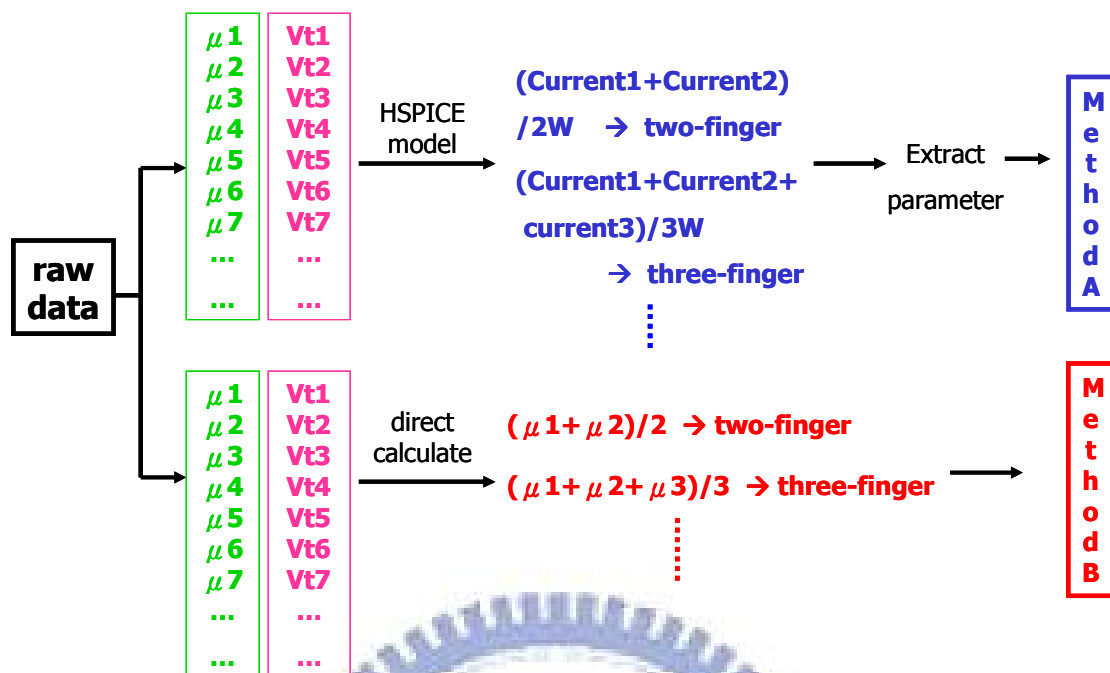
Fig. 4-4 This diagram shows the selected raw data and the two methods of simulation process, Method A and Method B.

$$y = \frac{\alpha}{\exp(\frac{1}{2}(\frac{x-\beta}{\gamma}))}$$
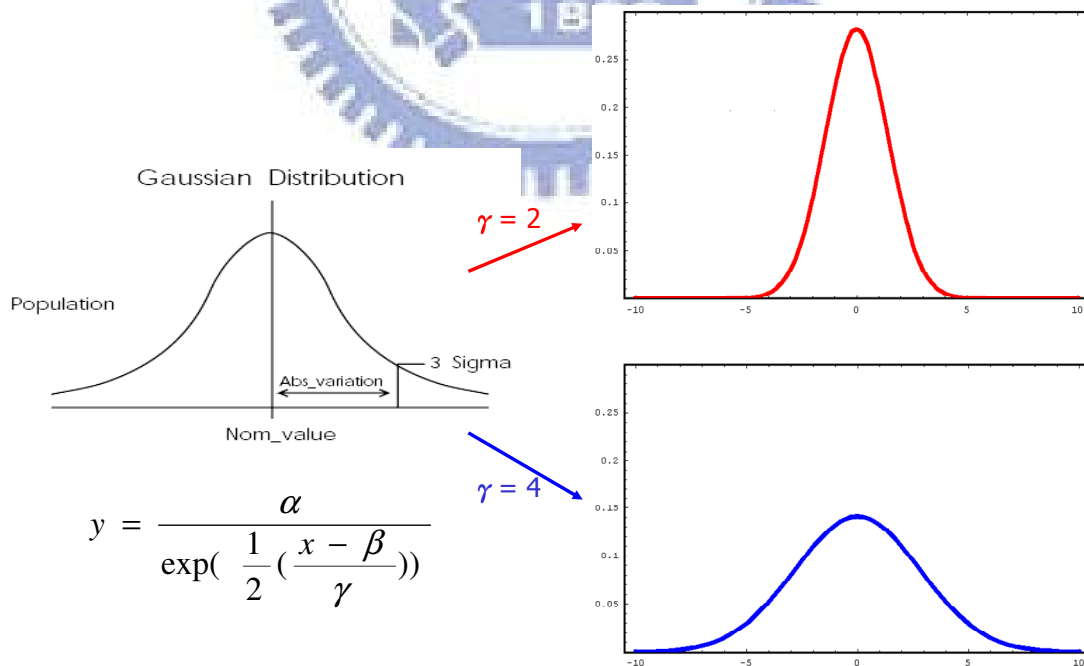
Fig. 4-5 The Gaussian distribution with different ranges, $\gamma = 2$ and $\gamma = 4$, where parameter "γ" stands for the standard deviation.
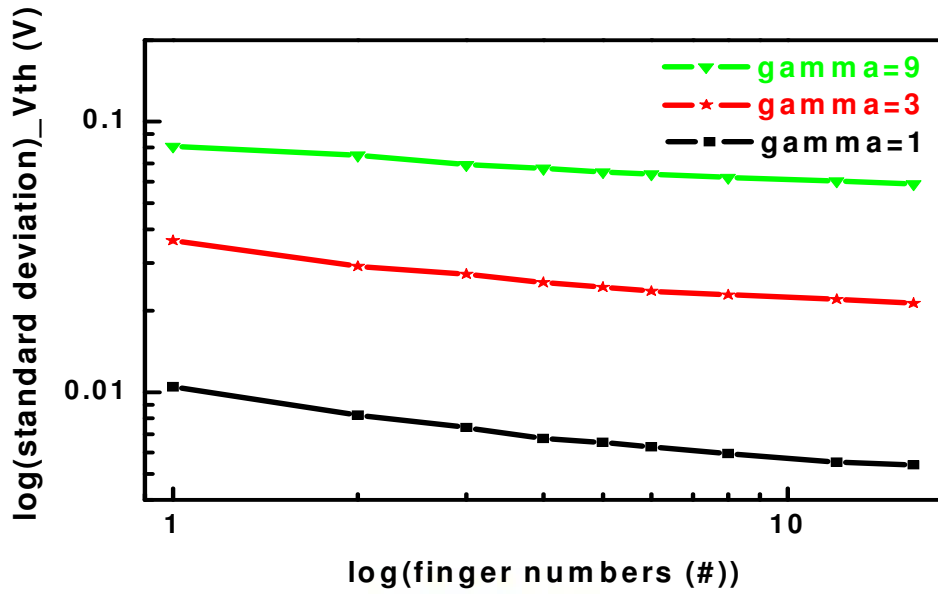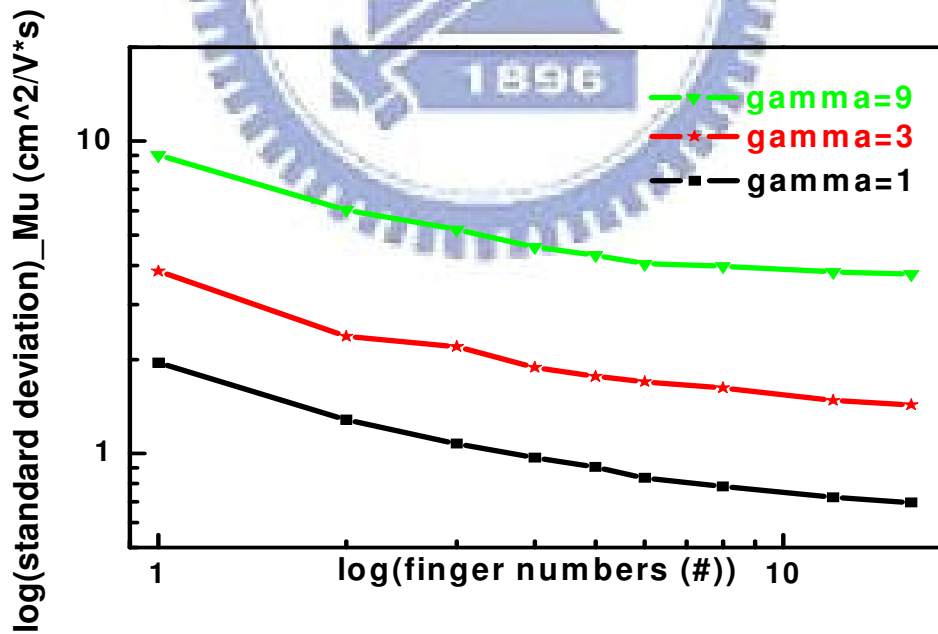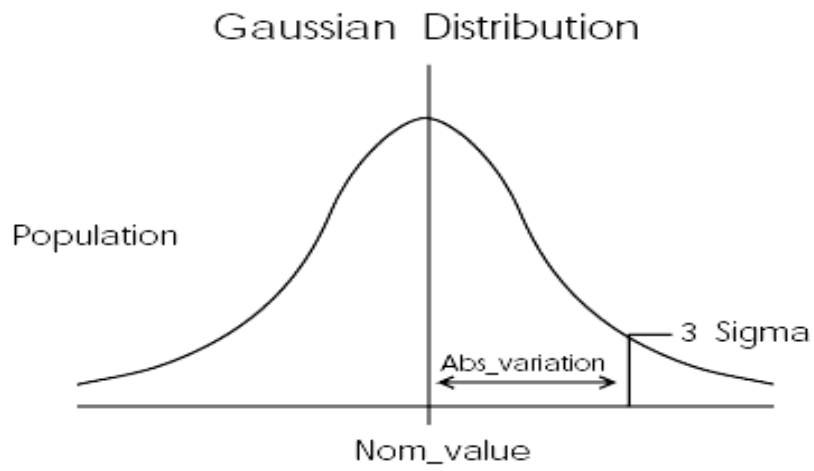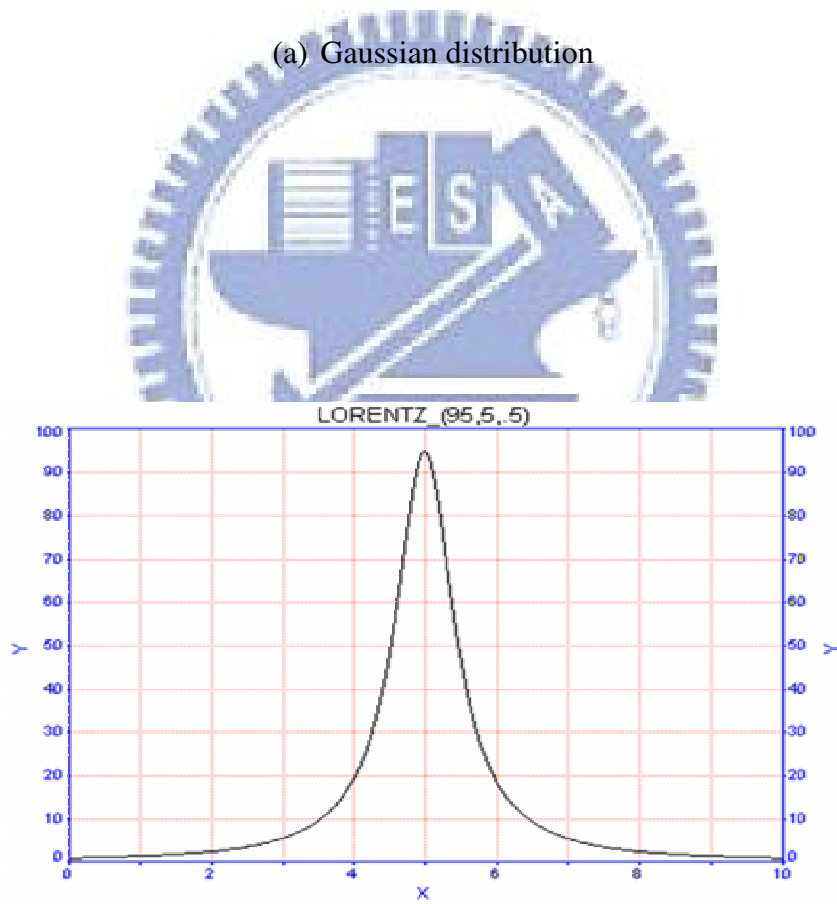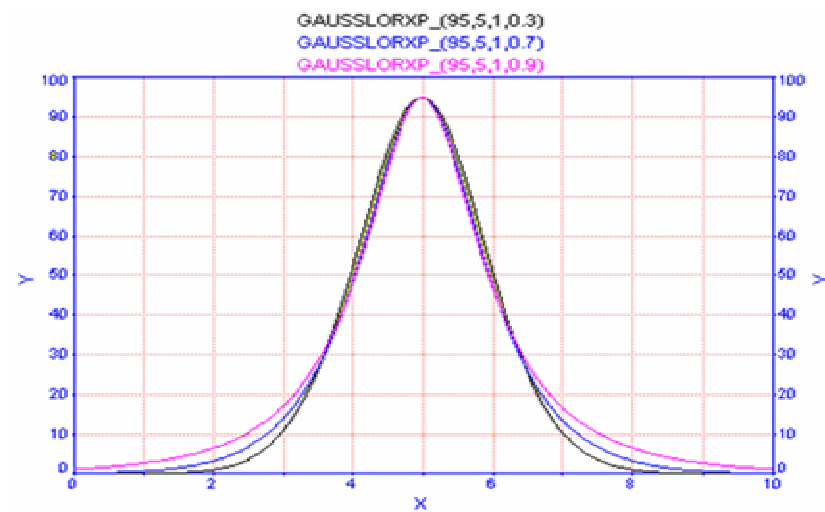
Fig. 4-6   Use Gaussian distribution to simulate the different range for Vth mismatch. The black, red and green lines respectively represent the standard deviation γ =1, γ =3 and γ =9.

Fig. 4-7   Use Gaussian distribution to simulate the different range for Mu mismatch. The black, red and green lines respectively represent the standard deviation γ =1, γ =3 and γ =9.
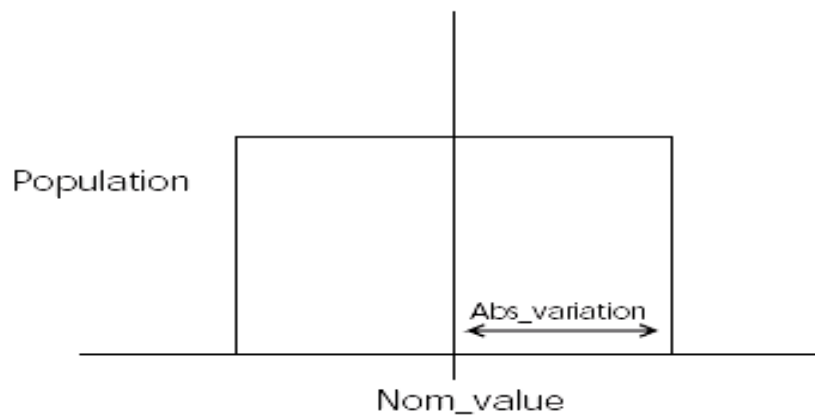
Gaussian Distribution

Population

3 Sigma

Abs_variation

Nom_value

(a) Gaussian distribution

LORENTZ_(95,5,.5)

(b) Lorentzian distribution

GAUSSLORXP_(95,5,1,0.3)
GAUSSLORXP_(95,5,1,0.7)
GAUSSLORXP_(95,5,1,0.9)

(c) Gauss-Lorentzian distribution

Uniform Distribution

Population

Abs_variation

Nom_value
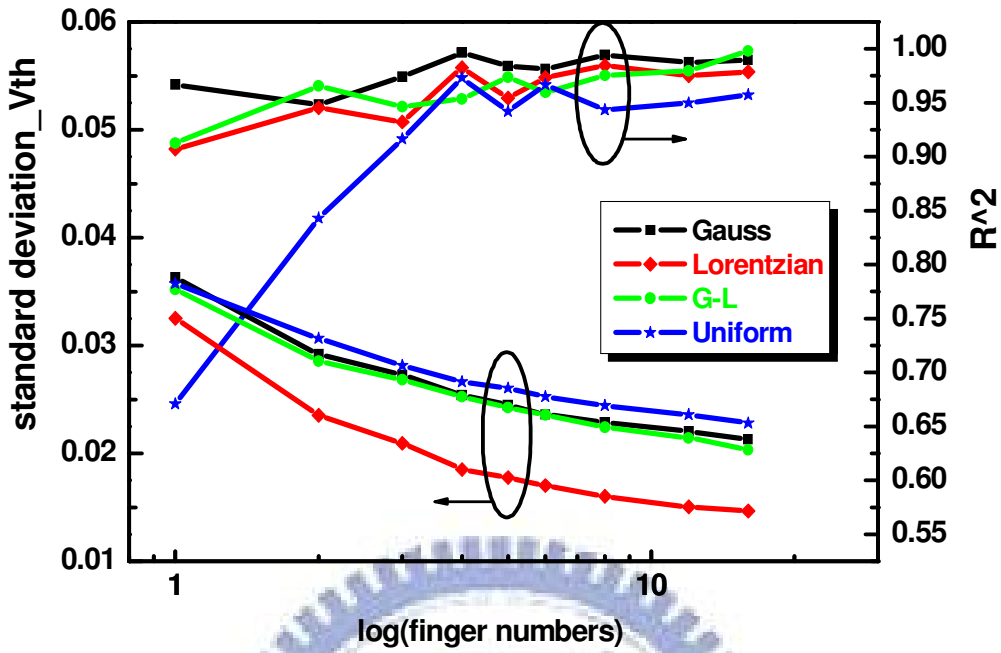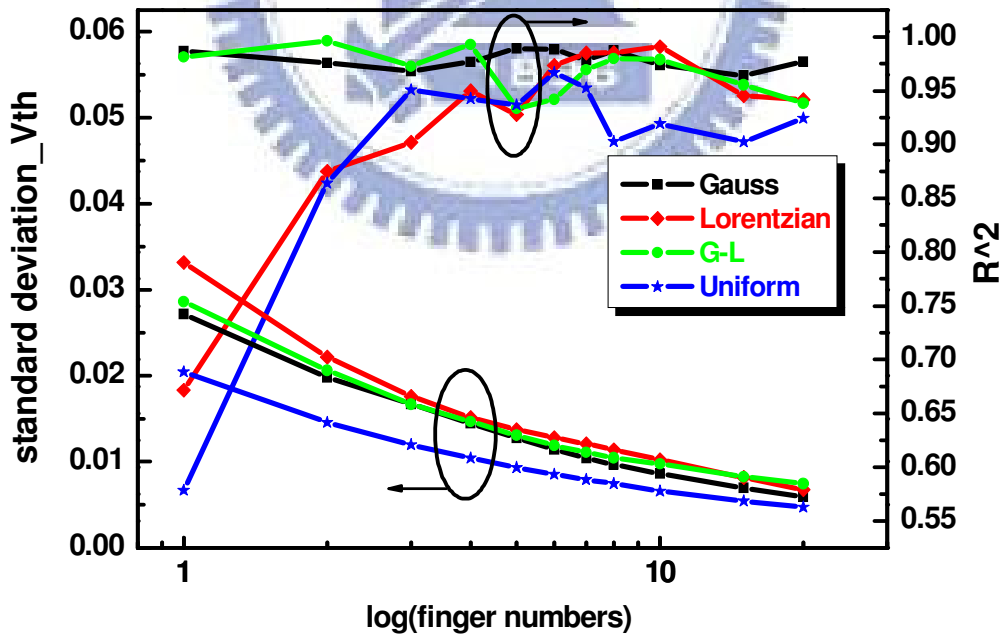
(d)Uniform distribution

Fig. 4-8 (a)Gaussian distribution (b)Lorentzian distribution (c)Gauss-Lorentzian
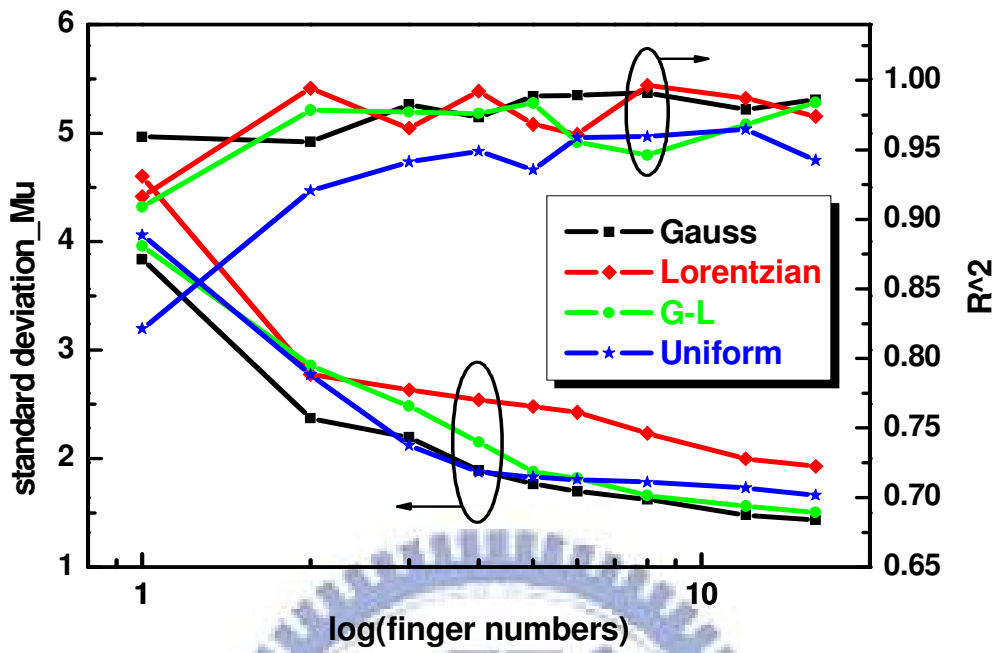
distribution (d)Uniform distribution.
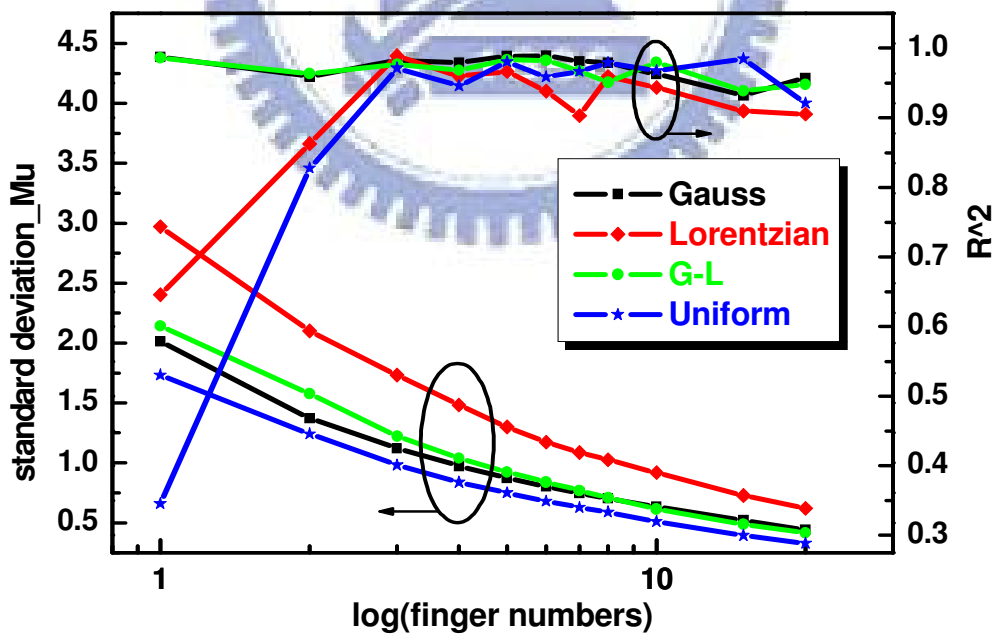
(a)Method A

(b)Method B

Fig. 4-9 The R square value on right vertical axis and the standard deviation on left

vertical axis for Vth of (a)Method A and (b)Method B.

(a)Method A

(b)Method B

Fig. 4-10 The R square value on right vertical axis and the standard deviation on left

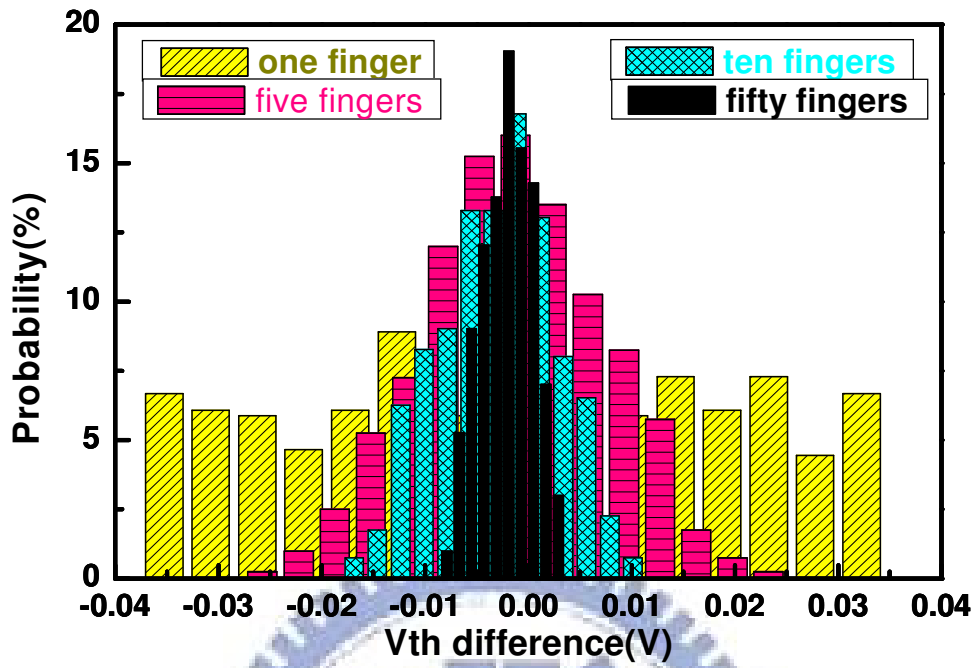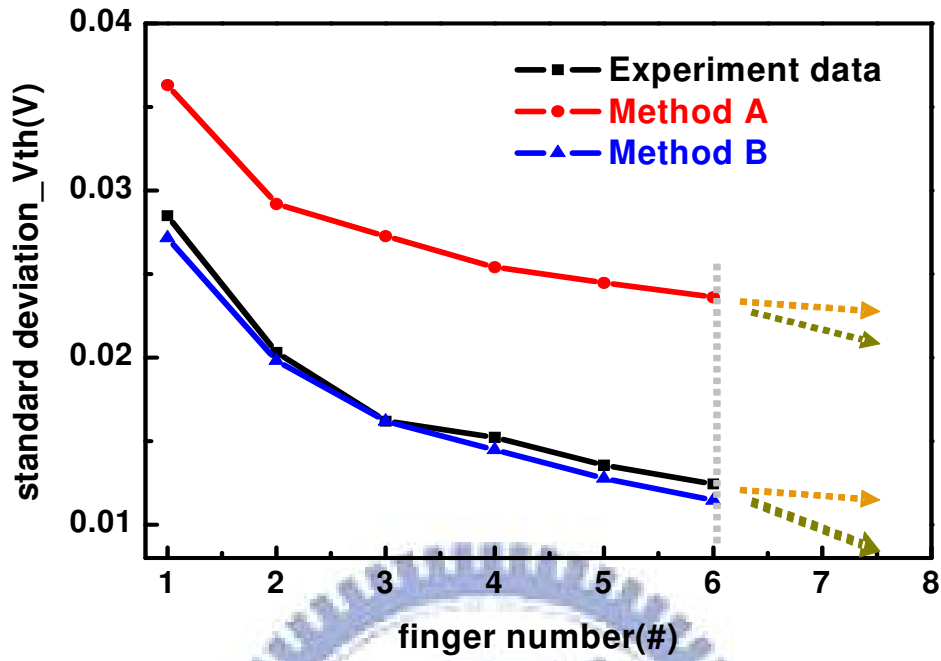vertical axis for Mu of (a)Method A and (b)Method B.

Fig. 4-11 The statistical diagram of the Uniform distribution for Method B with one-finger, five-finger, ten-finger and fifty-finger.

(a) mismatch of Vth
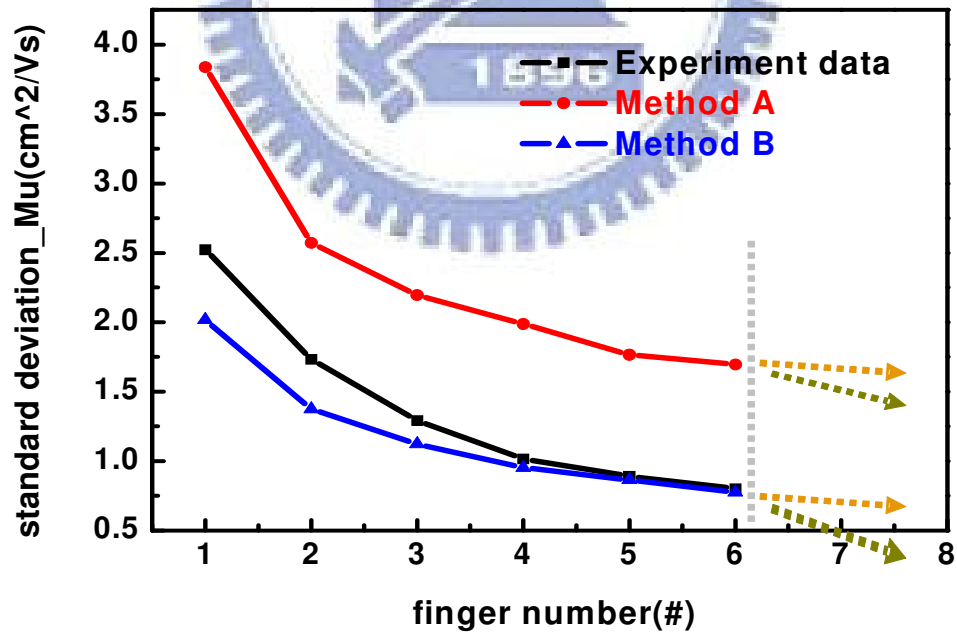
(b) mismatch of Mu

Fig. 4-12 The data of (a) Δ Vth and (b) Δ Mu of one-finger to six-finger from the

experiment and the simulation of Method A and Method B.

Fig. 4-13 The Vth mismatch of sixty-four-finger for Method A with the fitting

equations displayed inside the diagram.

Fig 4-14 The Mu mismatch of sixty-four-finger for Method A with the fitting

equations displayed inside the diagram.

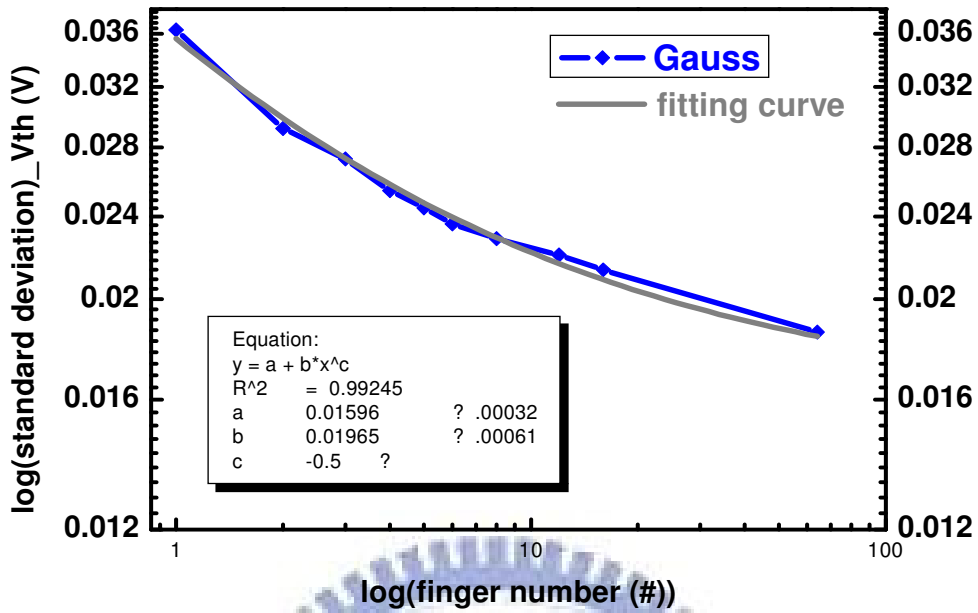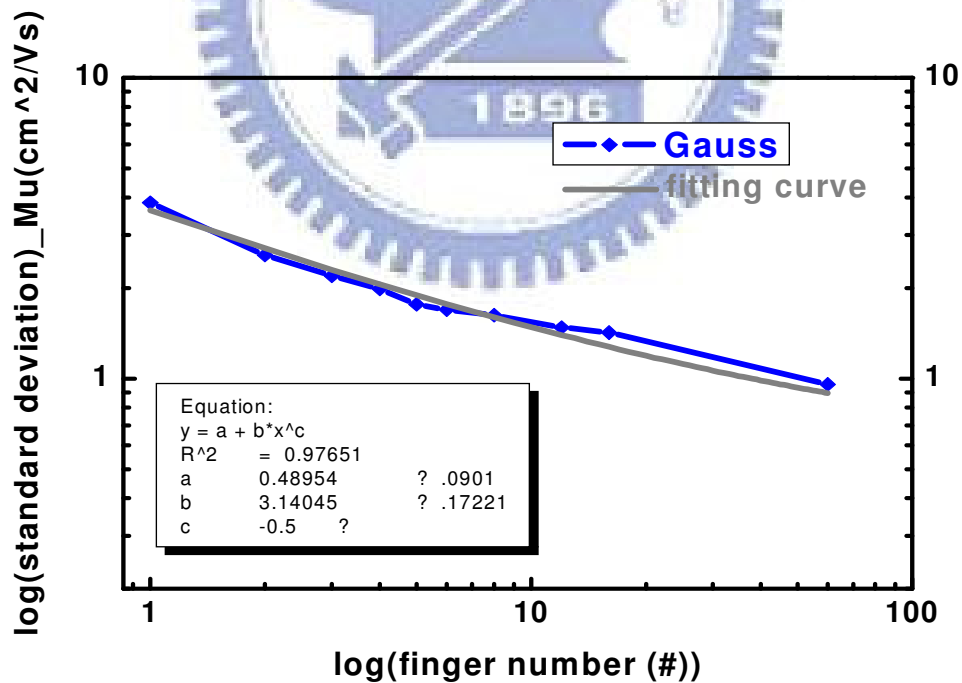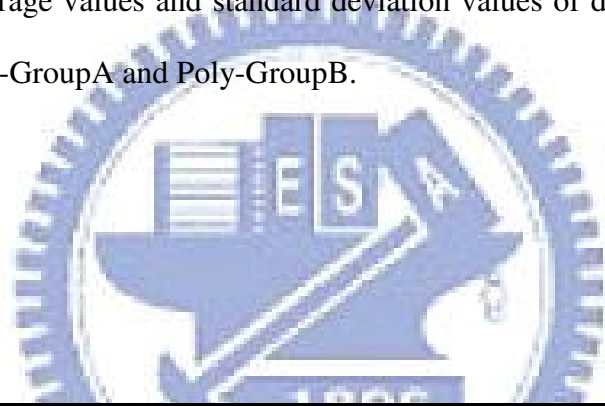| Device		Poly-GroupA		Poly-GroupB	
		N-type	P-type	N-type	P-type
Vth	Mean.	1.65	-2.39	1.69	-2.41
	Std.	0.019	0.024	0.03	0.05
Mu	Mean.	66.33	79.08	59.66	75.31
	Std.	1.70	1.61	7.84	2.29

Table3-1 The average values and standard deviation values of device parameters for the Poly-GroupA and Poly-GroupB.

Device (N-type)		Poly_GroupA		Poly_GroupB	
Standard Deviation		Vth (V)	Mu (cm^2/V*s)	Vth (V)	Mu (cm^2/V*s)
finger number	One-finger	0.0222	1.8108	0.0315	3.0237
	Two-finger	0.0154	1.3619	0.0239	2.3961
	Three-finger	0.0122	1.1585	0.0205	1.9764
	Four-finger	0.0106	1.0312	0.0185	1.7105
	Five-finger	0.0087	0.9765	0.0155	1.5268
	Six-finger	0.0082	0.9482	0.0135	1.3979

Table3-2 The standard deviation of $\triangle$Vth and $\triangle$Mu for n-type devices

Device (P-type)	Poly_GroupA		Poly_GroupB	
Standard Deviation	Vth (V)	Mu (cm^2/V*s)	Vth (V)	Mu (cm^2/V*s)
finger number — One-finger	0.02849	1.7043	0.0418	2.5223
Two-finger	0.02033	1.1776	0.028	1.7336
Three-finger	0.01621	0.9579	0.0255	1.2928
Four-finger	0.01523	0.8344	0.0223	1.0156
Five-finger	0.01356	0.7055	0.0204	0.8703
Six-finger	0.01244	0.6465	0.0184	0.8004

Table3-3 The standard deviation of △Vth and △Mu for p-type devices

Device		a	b	c	R^2
Poly-GroupA	△Vth_N type	-0.0017	0.0239	-0.5	0.9981
	△Vth_P type	0.0017	0.0269	-0.5	0.9959
	△Muo_N type	0.3081	1.4939	-0.5	0.9968
	△Muo_P type	-0.0765	1.7817	-0.5	0.9991
Poly-GroupB	△Vth_N type	0.0028	0.0293	-0.5	0.9812
	△Vth_P type	0.0029	0.0382	-0.5	0.9887
	△Muo_N type	0.3272	2.7660	-0.5	0.9866
	△Muo_P type	-0.4401	2.9878	-0.5	0.9868

Table3-4 The fitting parameter of the proposed model for the Poly-GroupA and

Poly-GroupB devices

Device	R^2	a	b
a-Si	0.8913	-0.0079	0.7961
Poly_A	0.9981	-0.0017	0.2394
Poly_B	0.9812	0.0028	0.2929
c-Si	1	-2.7E-7	0.0246

Table3-5 The fitting parameter of $\triangle$Vth with finger numbers for n-type different

devices

Device	R^2	a	b
Poly_A	0.9959	0.0017	0.2696
Poly_B	0.9887	0.0029	0.3813
c-Si	1	-9.0E-11	0.0019

Table3-6 The fitting parameter of $\triangle$Vth with finger numbers for p-type different
devices

Device	R^2	a	b
a-Si	0.9957	-4.7E-10	3.5E-8
Poly_A	0.9997	8.2E-11	3.9E-9
Poly_B	0.9867	9.5E-11	8.0E-9
c-Si	1	6.7E-15	4.2E-8

Table3-7 The fitting parameter of $\triangle$beta with finger numbers for n-type different
devices

Device	R^2	a	b
Poly_A	0.9991	-1.7E-11	3.9E-9
Poly_B	0.9968	-1.0E-10	6.9E-9
c-Si	1	-2.1E-18	3.3E-10

Table3-8 The fitting parameter of △beta with finger numbers for p-type different
devices

	γ =1	γ =3	γ =9
R^2	0.99525	0.9906	0.98769
a	0.00352	0.01587	0.05156
b	0.0068	0.01979	0.03058
c	-0.5	-0.5	-0.5

Table 4-1   The fitting parameters of the Vth mismatch for the simulation of different range.

	γ =1	γ =3	γ =9
R^2	0.96896	0.9462	0.94528
a	0.19015	0.47309	1.43642
b	1.6557	3.09548	7.02415
c	-0.5	-0.5	-0.5

Table 4-2 The fitting parameters of the Mu mismatch for the simulation of different range.

	Gauss	Lorentzian	Gauss-Lorentzian	Uniform
Equation	$y=\dfrac{\alpha}{\exp(\frac{1}{2}(\frac{x-\beta}{\gamma}))}$	$y=\dfrac{a}{1+(\frac{x-b}{c})^2}$	$y=\dfrac{a}{(1+d(\frac{x-b}{c})^2)*\exp((1-d)*\frac{1}{2}(\frac{x-b}{c})^2)}$	$P(x)=\begin{cases}0 & for & x<a\\ \dfrac{1}{b-a} & for & a\le x\le b\\ 0 & for & x>b\end{cases}$
Parameter	amplitude=α center=β constraints= γ	amplitude=a center=b constraints=c	amplitude=a center=b constraints: c>0, $0\ge d\ge 1$	amplitude=$\dfrac{1}{b-a}$ range= $a\le x\le b$

Table4-3 The equations and the parameters for the different distributions

fitting		Experiment data	Method A	Method B
Power law	R^2_Vth	0.995	0.995	0.998
	R^2_Mu	0.997	0.990	0.999
Exponential	R^2_Vth	0.9947	0.991	0.996
Law	R^2_Mu	0.999	0.992	0.997

Table 4-4 The R square values of the fitting parameters based on equation (3-1) and
exponential laws for the experiment data, and Method A, and Method B.